The Geological Society of America
Field Guide 15
2009

Geological and geophysical perspectives on the magmatic and tectonic development, High Lava Plains and northwest Basin and Range

Andrew Meigs*
Oregon State University, Department of Geosciences, Wilkinson 104, Corvallis, Oregon 97331, USA

Kaleb Scarberry
Colorado State University, Department of Geosciences, 322 Natural Resources Building, Fort Collins, Colorado 80523, USA

Anita Grunder
Oregon State University, Department of Geosciences, Wilkinson 104, Corvallis, Oregon 97331, USA

Richard Carlson
Carnegie Institution of Washington, Department of Terrestrial Magnetism, 5241 Broad Branch Road, NW, Washington, D.C. 20015, USA

Mark T. Ford
Oregon State University, Department of Geosciences, Wilkinson 104, Corvallis, Oregon 97331, USA

Matt Fouch
Arizona State University, School of Earth & Space Exploration, P.O. Box 871404, Tempe, Arizona 85287, USA

Tim Grove
Massachusetts Institute of Technology, Department of Earth, Atmospheric, & Planetary Sciences, 77 Massachusetts Avenue, Cambridge, Massachusetts 02139, USA

William K. Hart
Miami University, Department of Geology, Shideler Hall 114, Oxford, Ohio 45056, USA

Mike Iademarco
Oregon State University, Department of Geosciences, Wilkinson 104, Corvallis, Oregon 97331, USA

Brennan Jordan
University of South Dakota, Department of Earth Sciences, 414 E. Clark St., Vermillion, South Dakota 57069, USA

Justin Milliard
Oregon State University, Department of Geosciences, Wilkinson 104, Corvallis, Oregon, 97331, USA

*meigsa@geo.oregonstate.edu

Meigs, A., Scarberry, K., Grunder, A., Carlson, R., Ford, M.T., Fouch, M., Grove, T., Hart, W.K., Iademarco, M., Jordan, B., Milliard, J., Streck, M.J., Trench, D., and Weldon, R., 2009, Geological and geophysical perspectives on the magmatic and tectonic development, High Lava Plains and northwest Basin and Range, *in* O'Connor, J.E., Dorsey, R.J., and Madin, I.P., eds., Volcanoes to Vineyards: Geologic Field Trips through the Dynamic Landscape of the Pacific Northwest: Geological Society of America Field Guide 15, p. 435–470, doi: 10.1130/2009.fld015(21).

Martin J. Streck
Portland State University, Department of Geology, P.O. Box 751, Portland, Oregon 97207, USA

David Trench
Oregon State University, Department of Geosciences, Wilkinson 104, Corvallis, Oregon 97331, USA

Ray Weldon
University of Oregon, Department of Geological Sciences, 151 Cascade Annex, 1272 University of Oregon, Eugene, Oregon 97403, USA

ABSTRACT

A large part of the northwestern United States has undergone extensive late Cenozoic magmatic activity yielding one of the great continental volcanic provinces on Earth. Within this broader area lies the High Lava Plains province, the focus of this field guide. For our purposes, the High Lava Plains is a middle and late Cenozoic volcanic upland, contiguous with and gradational into the Basin and Range province to the south.

The High Lava Plains province of southeastern Oregon is characterized by thin, widespread Miocene-Pleistocene lava flows of primitive basalt and a belt of silicic eruptive centers. The rhyolitic rocks generally are successively younger to the northwest, describing a mirror image to the basalt plateau and rhyolite age progression of the Snake River Plain. The High Lava Plains is associated with a zone of numerous, small northwest-striking faults and lies at the northern limit of major Basin and Range normal faults. The abundant late Cenozoic bimodal volcanism occupies an enigmatic intracontinental tectonic setting affected by Cascadia subduction, Basin and Range extension, the Yellowstone plume, and lithospheric topography at the edge of the North American craton. The purpose of this field trip is to focus on the late Cenozoic lithospheric evolution of this region, through the lens of the High Lava Plains, by considering structural, geophysical, petrologic, and temporal perspectives.

A grand tour southeast from Bend to Valley Falls, north to Burns, and then east to Venator, Oregon, takes participants from the eastern edge of the Cascade volcanic arc, across several basins and ranges in eastern Oregon, and onto the volcanic plateau of the High Lava Plains. Day 1 provides an overview of Newberry Volcano and the western edge of Basin and Range, including the Ana River and Summer Lake fault zones. On Day 2, the early magmatic and extensional history of the region is explored along the Abert Rim range-front fault. Participants are introduced to the bimodal volcanism within the High Lava Plains, with focus on the Harney Basin and Rattlesnake ignimbrite event. An evening session will highlight geophysical results from the High Lava Plains, including new data from one of the largest active-source seismic experiments to be conducted in North America. Day 3 activities examine early bimodal volcanic history of the eastern High Lava Plains and the late Miocene and Pliocene subsidence history on the east edge of the Harney Basin east of Burns, Oregon.

GEOLOGIC SETTING OF THE HIGH LAVA PLAINS

The Crust

The High Lava Plains province of eastern Oregon is bounded to the north by the non-extended Blue Mountains province, to the south by the Basin and Range, to the west by the Cascade Range and to the east by Precambrian North America (Fig. 1). In this area, the western margin of the Precambrian North American craton is well delineated only along the western Idaho shear zone, a steep structural boundary near the Idaho-Washington border that is coincident with an abrupt change in the initial $^{87}Sr/^{86}Sr$ of Mesozoic and Cenozoic magmatic rocks from <0.706 west to >0.706 east of the western Idaho shear zone (Armstrong et al., 1977; Manduca et al., 1992). Elsewhere, the location of the Proterozoic cratonic margin is more enigmatic but can be inferred from the location of the "0.706 line" (Fig. 1). Pre-Cenozoic crust west of the craton margin is exposed in

northeastern and central Oregon and westernmost Idaho and consists of Paleozoic-Mesozoic oceanic volcanic arcs, accretionary prism complexes, and associated basinal successions accreted to western North America during Jurassic arc-continent collision (e.g., Coney and Reynolds, 1977; Dickinson, 1979; Oldow et al., 1984; Vallier, 1995). Similar terranes are exposed in the Klamath Mountains of southwestern Oregon and northern California. If such basement exists under the High Lava Plains, it is covered by Cenozoic volcanic rocks.

From a seismic refraction transect along the High Lava Plains, Catchings and Mooney (1988) inferred a Moho depth of 37 km and high seismic velocity (7.4 km/s) in the lower crust. Preliminary receiver function analysis of Moho depths beneath the High Lava Plains seismic array shows the following systematic variations (K.C. Eagar, 2009, pers. commun.). Crustal thicknesses beneath the High Cascades are ~40–42 km, but diminish abruptly to ~30 km in the westernmost High Lava Plains. These depths gradually increase to ~35 km to the east beneath Jordan Craters, and then increase dramatically to ~42 km and perhaps thicker beneath the Owyhee Plateau.

Regional Volcanism

Western North America has experienced aerially extensive, voluminous volcanism throughout the Cenozoic that can be separated into three phases: the "ignimbrite sweep," characterized by large-volume eruptions of silicic magmas from centers migrating over much of western North America between 50 and 20 Ma (e.g., Lipman et al., 1972); the flood basalt episode between 17 and 15 Ma that involved the massive emplacement of dikes and the eruption of flood basalt along a ~700-km-long, north-south line that follows the western margin of Precambrian North America (e.g., Hooper et al., 1997); and finally, more distributed and generally bimodal (silicic and basaltic) volcanism along the margins of the Basin and Range (Fig. 1). During the third, still continuing, phase, the largest volumes of magma were erupted in the High Lava Plains and along the Snake River Plain. By ca. 12 Ma, volcanism in eastern Oregon became more clearly organized to form two migrating tracks, one moving at plate speed and plate direction to the northeast along the Snake River Plain toward Yellowstone (Pierce and Morgan, 1992) and the other moving in the

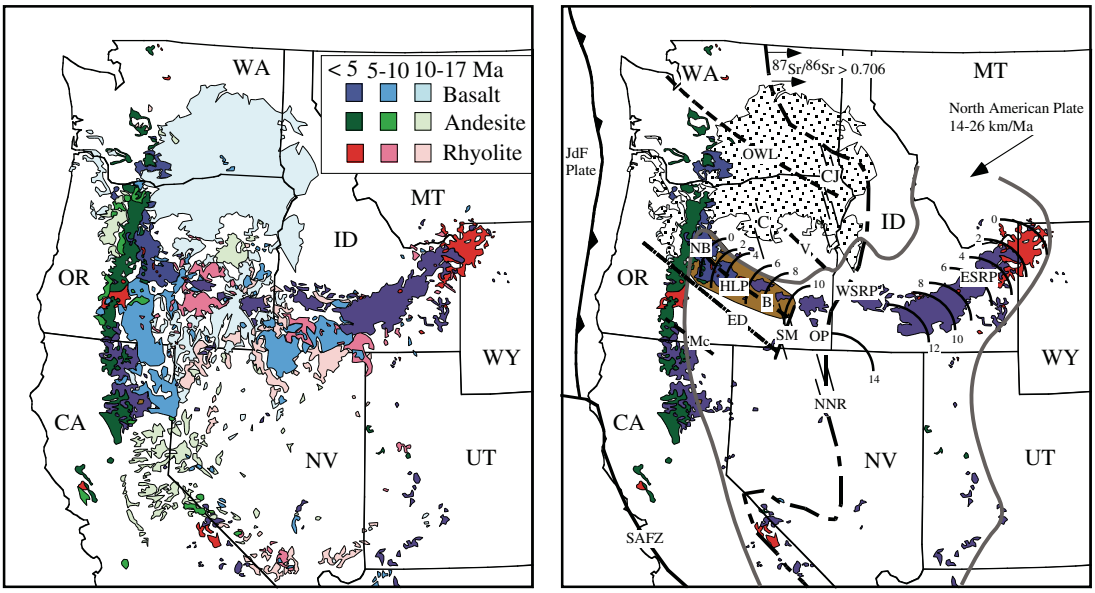

Figure 1. Volcanic and tectonic elements of the western United States: (A) Distribution of volcanic rocks younger than 17 Ma, by age and composition (Luedke and Smith, 1984), illustrates the tremendous volcanic activity east of the Cascade Range in the northern extent of the Basin and Range province. (B) Some tectonic elements (after Jordan et al., 2004) superimposed on the map of Luedke and Smith (1984). Solid brown line outlines the Basin and Range province. Volcanic fields younger than 5 Ma illustrate the continuing activity in the Cascade Range and along the High Lava Plains (HLP; brown field) and the eastern Snake River Plain (ESRP). Short curves along the HLP and ESRP are isochrons (ages in Ma) for the migrating silicic volcanism along each volcanic trace. Flood basalt activity was fed from dike systems in the northern Nevada rift (NNR), Steens Mountain (SM), the western Snake River Plain (WSRP) and the Chief Joseph (CJ) and Cornucopia (C) dike swarms of the Columbia River Basalt Group. These dikes occur near the western border of Precambrian North America as defined by the $^{87}Sr/^{86}Sr$ 0.706 line (large dot-dash line). Northwest-trending fault systems—Olympic-Wallowa lineament (OWL), Vale (V), Brothers (B), Eugene-Denio (ED) and McLoughlin (Mc)—are shown by the short-dashed lines. Additional features include Newberry Volcano (NB), Owyhee Plateau (OP), Juan de Fuca Plate, San Andreas fault zone (SAFZ), and Mendocino triple junction (MTJ).CA—California; ID—Idaho; OR—Oregon; NV—Nevada; UT—Utah; WA—Washington; WY—Wyoming.

opposite direction (west-northwest) at a similar rate along the High Lava Plains (Jordan et al., 2004; MacLeod et al., 1975). The spatio-temporal progression is defined by silicic volcanism, which is estimated to be about ten times less voluminous along the High Lava Plains than along the Yellowstone track (Pierce et al., 2000). The migrating silicic volcanism of the High Lava Plains ends today near Newberry Volcano (Fig. 2), an active volcano of the Cascade volcanic arc. At the latitude of Newberry and the Three Sisters, the Cascade arc has unusually abundant Quaternary mafic volcanic rocks owing to youthful intra-arc rifting and has a fairly thin (35–42 km) and mafic crust (Conrey et al., 2000; Sherrod and Smith, 1990; Trehu et al., 1994). A link between volcanism in the High Lava Plains and the Cascades is indicated by enhanced volcanic output of the Cascade Range from Crater Lake to Mount Jefferson, isotopic similarity of primitive low-K tholeiites, and a westward merging of High Lava Plains structures with the High Cascades graben.

Unlike the silicic activity, basaltic volcanism of the High Lava Plains is not age-progressive. Instead, it changed from widely distributed in the Miocene to focused in the Pliocene to define the geomorphic High Lava Plains (Fig. 1). There was a prominent pulse of basaltic activity all across the High Lava Plains at ca. 7.5–8 Ma (Jordan et al., 2004). After passage of the silicic volcanic front, volcanism persisted along both tracks, erupting primarily basalt to the present day along most of the High Lava Plains and Snake River Plain. Inasmuch as silicic volcanism is driven by mafic volcanism, there may be an age progression superimposed on the near 7.5–8 Ma basaltic burst.

With the beginning of the High Lava Plains activity, basaltic volcanism shifted from the large-volume eruptions of differentiated basalt that typify the Steens–Columbia River flood basalt to primarily primitive, low-K, high-Al, olivine tholeiite (HAOT of Hart, 1985) that shares many compositional similarities with mid-ocean ridge basalt. This type of primitive basalt occurs throughout eastern Oregon (Conrey et al., 1997; Hart et al., 1984; McKee et al., 1983), along the Snake River Plain to Yellowstone (Leeman, 1982), and at various centers in the Cascade Range (Bacon et al., 1997) but is essentially absent in the central and southern Basin and Range (Nevada to Arizona). Experimental petrologic investigations of HAOT from the Cascade Range give a shallow mantle equilibration depth of 1.1 GPa (11 kbar) (Bartels et al., 1991) indicating that HAOT equilibrated close to the base of the crust (~33 km depth). Seismic tomography under the High Lava Plains (Roth et al., 2008) shows well-developed regions of low seismic velocity beneath surface expressions of recent volcanism that extend to depths of only 100–150 km, in agreement with the shallow origin of the volcanism indicated by the petrology of the basalts.

The <12 Ma rhyolites of the High Lava Plains and adjacent regions of the northwestern most Basin and Range Province are mainly high-silica rhyolites with >72 wt% SiO_2 (Figs. 3 and 4; Table 1) They fall into three general compositional groups. (1) Fe-rich rhyolites are essentially restricted to the basalt plateau of the High Lava Plains. The Rattlesnake Tuff is of this group. These rhyolites are closely tied to basalt in space and composition and have their origin mainly as partial melts of a mafic crust followed by extensive crystal fractionation to make the most evolved members of the suite (Streck and Grunder, 2008). Some of these may also be simple basalt fractionates as demonstrated for similar rhyolites on the Snake River Plain (Ford et al., 2004; McCurry et al., 2008; Whitaker et al., 2008). On the whole, this group coincides with Fe-Ca distribution comparable to rift zone rhyolites of Iceland (Fig. 3) (Jónasson, 2007). (2) Calcic rhyolites are widely distributed, have chemical affinities with the Cascades (particularly Medicine Lake Volcano), and may have their origin as extracts from granitoid crystal mushes (Bachmann and Bergantz, 2004; Hildreth, 2004). (3) Alkalic, and in some instances substantially peralkaline rhyolites, are found mainly in the central High Lava Plains.

Active Tectonics of the Northwestern Basin and Range

A variety of data suggest that the Cascadia forearc, or the central Oregon block, is moving westward and northward about a pole located in northeast Oregon or eastern Washington (Wells

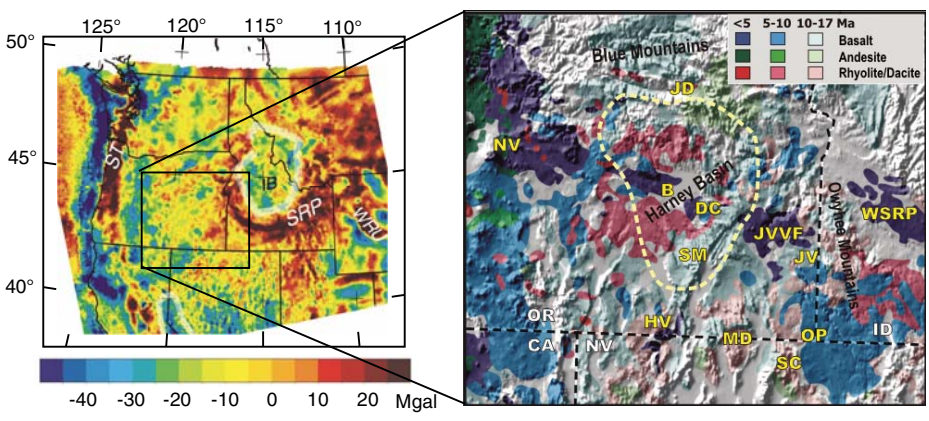

Figure 2. Residual isostatic gravity anomaly map for the northwestern U.S. (Keller et al., 2002). The expanded map to the right shows the general volcanic geology depicted in Figure 1 draped over a digital elevation model of southeast Oregon. Dashed outline depicts the approximate extent of the Devine Canyon Ash-Flow Tuff. Abbreviations in yellow are: NV—Newberry Volcano; JD—John Day; B—Burns; DC—Diamond Craters; SM—Steens Mountain; HV—Hawkes Valley volcanic field; MD—McDermitt volcanic field; JVVF—Jordan Valley volcanic field; JV—Jordan Valley; SC—Santa Rosa–Calico volcanic field and northern part of northern Nevada rift; OP—Owyhee Plateau; WSRP—western Snake River Plain.

TABLE 1. REPRESENTATIVE RHYOLITE COMPOSITIONS FROM THE HIGH LAVA PLAINS (HLP) AND SOUTHEASTERN OREGON (FIG. 3) NORMALIZED TO 100% ANHYDROUS

Location	RST A HLP most evolved	RST E HLP least evolved	Horse Mountain HLP peralkaline	Quartz Mountain HLP Fe-rich	Roundtop Butte HLP calcic (low Fe)	Cox Flat NWBR calcic (low Fe)
Age (Ma)	7.05	7.05	7.096	1.13	~6.5	8.05
SiO_2	77.74	75.64	76.49	75.51	76.29	76.71
TiO_2	0.11	0.16	0.20	0.103	0.07	0.061
Al_2O_3	11.97	12.29	10.43	13.39	13.41	13.46
FeO*	0.78	1.96	3.25	1.45	0.57	0.49
MnO	0.08	0.10	0.10	0.038	0.06	0.070
MgO	0.05	0.01	0.00	0.05	0.00	0.05
CaO	0.26	0.50	0.18	0.89	0.81	0.84
Na_2O	3.46	4.62	4.83	4.49	4.02	3.57
K_2O	5.53	4.70	4.50	4.07	4.77	4.75
P_2O_5	0.02	0.01	0.02	0.013	0.01	0.008
AT	99.90	99.50	99.10	99.12	99.09	97.08
Rb (ppm)	122	64	122.6	129.0	131	142.4
Ba	39	1835	175	922	332	47
Sr	2.1	23.4	0.5	60	31	27
Zr	175	457	733	173	67	59
Nb	39.4	26.4	40.7	8.11	12.8	10.92
$^{87}Sr/^{86}Sr$	0.70499	0.70431	0.70320*	0.70440	~0.7045	0.70628
$^{143}Nd/^{144}Nd$	0.51284	0.51282	0.512860		0.512910	0.512860
$^{206}Pb/^{204}Pb$	18.849	18.847	18.8608	19.0620		18.7560
$^{207}Pb/^{204}Pb$	15.620	15.622	15.5983	15.6217		15.5914
$^{208}Pb/^{204}Pb$	38.535	38.547	38.5203	38.7146		38.4091

Note: Cox flat is a sample from the northwest Basin and Range (NWBR). Rattlesnake tuff samples are RST. AT indicates analytical totals. Data from Streck and Grunder (2008) and Ford and Grunder (unpublished).

*Due to very high Rb/Sr ratios, the initial value cannot be accurately calculated with the given age precision.

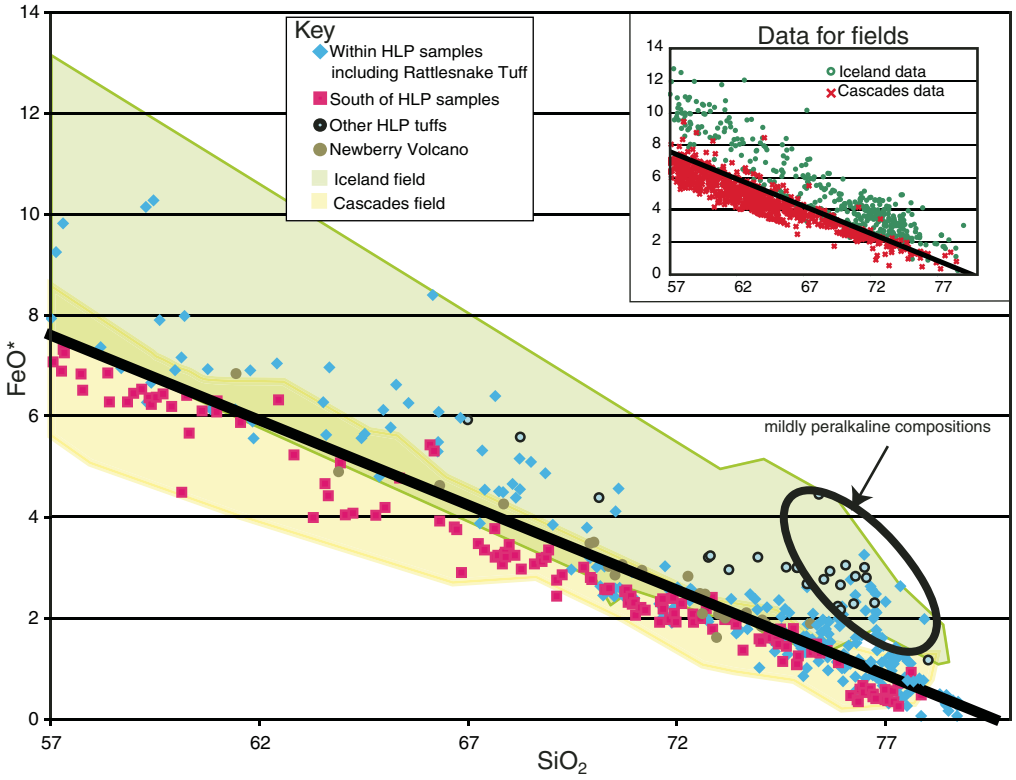

Figure 3. FeO* versus SiO_2 plot for samples >57% SiO_2 of the High Lava Plains (HLP) with an arbitrary dividing line between the more tholeiitic samples from the physiographic HLP, including voluminous tuffs, and the more calc-alkaline samples of the northern Basin and Range (cf. Christiansen and McCurry). Also shown are samples from Newberry Volcano and fields representing >425 samples from Iceland and >900 samples from the Cascades along with an inset showing these data points. The line nicely separates HLP and Basin and Range (south of the HLP samples) andesite to low silica rhyolite (57–72 wt% SiO_2) compositions but does not distinguish high silica rhyolites. High silica rocks of the study area are also not readily separated in other element variation diagrams a characteristic that has been noted in other provinces (e.g., Snake River Plain by Christiansen and McCurry, 2008). Mildly peralkaline compositions occur within the ellipse.

et al., 1998). Global Positioning System (GPS) and paleomagnetic studies (Hammond and Thatcher, 2005; McCaffrey et al., 2000; Wells and Simpson, 2001) have suggested three different Euler pole locations to accommodate the western and northward movement of the central Oregon block and the subsequent extension of central Oregon (Fig. 5). McCaffrey et al. (2000) use geodetic data to place a best-fit pole for the rotation of the central Oregon block at 45.9° ± 0.6° N, 118.7° ± 0.7° W, lying on the Oregon-Washington border. Wells and Simpson (2001) also resolve a pole of rotation for the Oregon coastal block along the Oregon-Washington border at 45.54° N, 119.60° W, but do so from geologic and paleomagnetic data, independent of geodetic data. The two-sigma error for the major axis of the pole is 5.1° along a 010° azimuth, with the minor axis at 2.96° (Wells and Simpson, 2001). Hammond and Thatcher (2005) place the Euler pole for the central Oregon block in northern Oregon, at 44.3° N, 118.04° W.

Implications for the instantaneous velocities and thus the magnitude of extension across the northwest Basin and Range

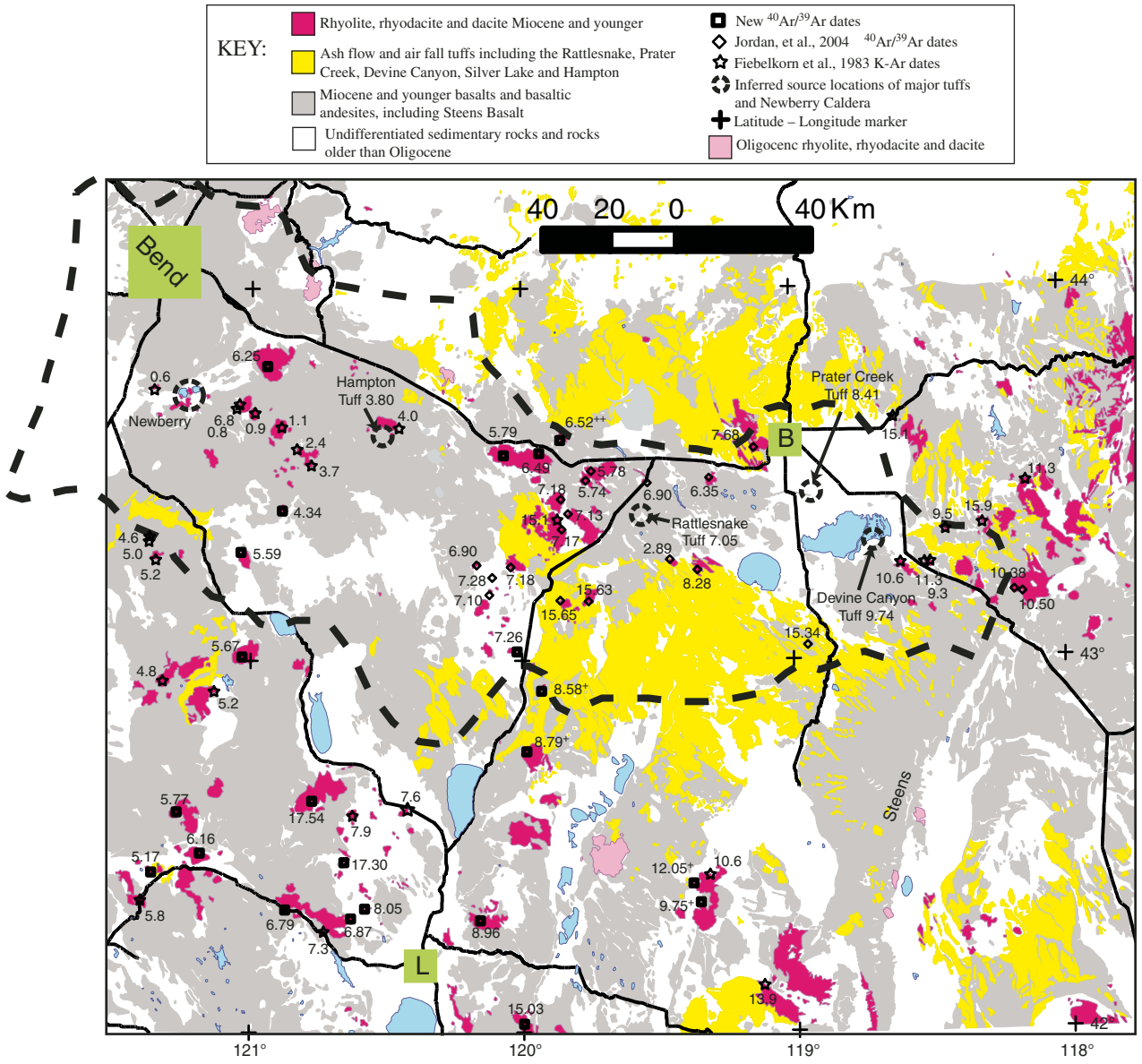

Figure 4. Map of eastern Oregon showing the spatial distribution of basalts and rhyolite lavas and tuffs. The location of 21 new $^{40}Ar/^{39}Ar$ ages are given (solid squares, reported to two decimals) including four unpublished ages of Scarberry et al. (2009) (+ symbol), ages from Jordan et al. (2004; $^{40}Ar/^{39}Ar$ ages, dark diamonds, reported to two decimals), and Fiebelkorn et al. (1983; K-Ar ages, open stars, reported to one decimal). Green boxes approximate cities (B—Burns, L—Lakeview). Proposed location for the Rattlesnake Tuff from Streck and Grunder (1997) and Ar-Ar age for the Hampton Tuff from Iademarco (2009). Black lines are major roads and heavy black dashed line outlines the High Lava Plains physiographic province.

vary depending on the location of the Euler pole for the central Oregon block. A pole along the Oregon-Washington border implies an instantaneous velocity in the Brothers fault zone and the northwest Basin and Range of ~5 mm/yr of westward motion relative to stable North America (McCaffrey et al., 2000; Wells and Simpson, 2001). A similar extension rate of 6 mm/yr was estimated by Pezzopane and Weldon (1993) based on geologic deformation in the region. Hammond and Thatcher (2005) suggest an Euler pole in Oregon, which implies an instantaneous velocity of 2 mm/yr of westward motion for the Brothers fault zone and the northwest Basin and Range relative to stable North America. An instantaneous value of 2 mm/yr lies within the uncertainties of GPS measurements and essentially results in a possible range of 0–2 mm/yr for Basin and Range extension in Oregon at a latitude of 43° N. Extension rates increase to the south toward Nevada (Hammond and Thatcher, 2005).

An Euler pole for the central Oregon block in southeast Oregon, or along the Oregon-Washington border, implies a decreasing velocity gradient moving from south to north approaching the pole. Measurements of active deformation in the Basin and Range indicate instantaneous velocities relative to stable North America decreasing from ~14 mm/yr near 35° N to ~2 mm/yr approaching the northwest Basin and Range near 41° N (Bennett et al., 2003; Miller et al., 2001). A south-increasing velocity gradient implies concomitantly greater magnitude of extension to the south away from the pole. Kinematically, a clockwise rotation of the central Oregon block and the attendant extension across the province requires a component of strike-slip motion across central Oregon to accommodate the block rotation and the boundary between less extended crust to the north and extended crust to the south (Fig. 5).

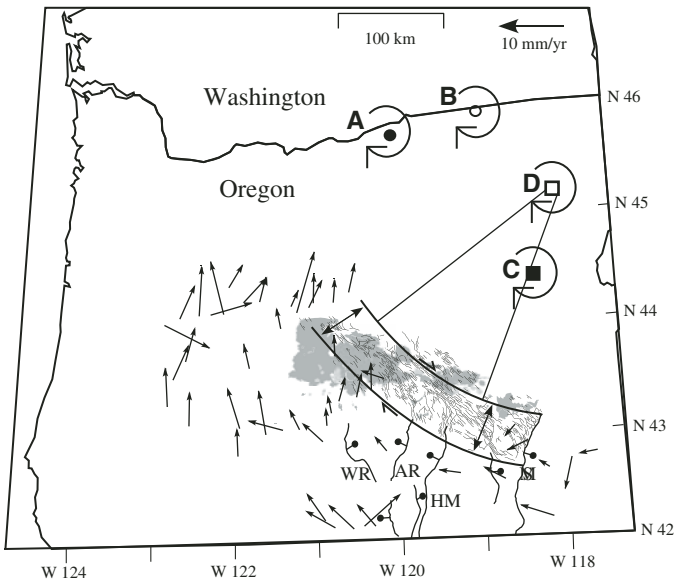

Figure 5. Working regional tectonic model for the Brothers fault zone and the northwest Basin and Range (from Trench, 2008). Possible Euler pole locations for the central Oregon block labeled as follows: A—pole defined by Wells and Simpson (2001); B—pole defined by McCaffrey et al. (2000); C—pole defined by Hammond and Thatcher (2005); D—approximate pole defined by lines tangential to the area of the Brothers fault zone. Arrows show motion vectors from campaign-style GPS surveys 1998–2003 (Hammond and Thatcher, 2005); error ellipses (not shown) for stations in and immediately south of the Brothers fault zone generally equal the signal. Shaded areas—Quaternary basalt; thick lines—large-separation (>150 m) fault escarpments; thin lines—small separation (<150 m) faults; WR—Winter Ridge; AR—Abert Rim; HM—Hart Mountain; SM—Steens Mountain (Jordan et al., 2004, McCaffrey et al., 2000).

Regional Structure

The post-Laramide structural evolution of the western plate boundary of the North American Plate was accompanied by magmatism and the development of the Basin and Range Province (c.f., Armstrong and Ward, 1991; Christiansen and Yeats, 1992; Wernicke, 1992). Deformation at the western margin of the Basin and Range since ca. 10 Ma is characterized by east-west extension and right-lateral shear (Zoback, 1989) coupled to the motion of the Pacific Plate, which has moved north-northwest at a rate of ~52 mm/yr, with respect to North America since ca. 8 Ma (Atwater and Stock, 1998). Numerous models suggest that forces driving the deformation include: (1) trench pull and subduction zone rollback due to removal of the Farallon slab underneath North America (Humphreys, 1995; Zandt and Humphreys, 2008); (2) rotation of the Cascadia forearc (c.f., Wells and Heller, 1988); (3) development and propagation of the two principal dextral fault systems of the plate boundary, the San Andreas (Atwater and Stock, 1998) and Walker Lane (Faulds et al., 2005; Wesnousky, 2005); and (4) collapse of the crust driven by gravitational potential energy due to thickening of the Laramide crust (Humphreys and Coblentz, 2007).

Structurally, the High Lava Plains is dominated by a wide, diffuse zone of northwest-striking faults, the Brothers fault zone, which has been interpreted as an intracontinental transform fault separating the Basin and Range Province from nonextended crust to the north (Fig. 6) (Lawrence, 1976). These northwesterly faults are mainly vertical, typically a few kilometers long, and have throws of only a few tens of meters (Lawrence, 1976; Trench, 2008; Walker and MacLeod, 1991). The Brothers fault zone and the High Lava Plains cross at an acute angle. In contrast, major Basin and Range faults strike north-northwest to north-northeast, are tens of kilometers long, are widely spaced, have throws on the order of kilometers, and bound the grabens. Differentiating "Basin and Range" from "Brothers or High Lava Plains" faults on the basis of trend is not wholly satisfying because faults of both trends occur in each structural province. Faults parallel to those of the Brothers fault zone are widely distributed in southeastern Oregon and have been grouped into northwest-trending tracts (for example, Figure 1B, Eugene-Denio zone), although these are not readily separable (Lawrence, 1976). GPS data identify a point on the central Oregon-Washington border as the rotation axis for extension that increases southward into the Basin and Range (c.f., McCaffrey et al., 2000). Paleomagnetic data suggest that eastern Oregon has been extended by ~17% during the past 15 Ma (Wells and Heller, 1988).

An understanding of the development and kinematics of the fault pattern in the High Lava Plains–northwest Basin and Range, in the context of plate boundary and body forces, has been limited by our poor knowledge about the timing of structural features across the region. In Oregon, faults occur with two principal orientations, north-northeast– and northwest-striking (Crider, 2001; Donath, 1962; Pezzopane and Weldon, 1993), and faults of each trend cut contemporaneous volcanic strata (Donath, 1962) (Fig. 6). North-, northwest-, and north-northeast–striking, Basin and Range–type faults bound the major topographic escarpments and have the greatest post-middle Miocene stratigraphic separation. Northwest-striking, High Lava Plains–type faults, in contrast, exhibit lower topographic and presumably structural relief. Geomorphic and paleoseismic observations indicate both fault sets are active (Pezzopane and Weldon, 1993). A variety of data, including analog experiments, dike orientations, cinder cone alignments, slip vectors from earthquake moment tensors, and moderate earthquakes, indicates that the fault sets in the region have formed in response to right-oblique extension toward N60°–70°W (see summaries in Pezzopane and Weldon, 1993, and Crider, 2001). A regional, pre-Miocene structural fabric may control the orientation of northwest-trending fault sets (c.f., Donath, 1962; Wells, 1980).

Timing and Style of Extension on North-Northeast– and Northwest-Striking Faults

Extension in the northwestern corner of the Basin and Range is variable in time. Scarberry et al. (2009) argue that the Coleman Hills volcanic center (ca. 22 Ma) formed along a northwest-trending structural fabric that influenced later development of the Abert Rim fault system. Near the southern end of the Steens Mountain range-front fault, 120 km farther east, an angular unconformity between the Steens Basalt and underlying volcanic and volcaniclastic rocks indicates tilting between 5° and 20° prior to 16.6 Ma (Langer, 1991; Minor et al., 1987). Motion on the northern part of the Steens Mountain range-front fault coincided with volcanic activity ca. 10 Ma (Johnson and Grunder, 2000), and the 9.7 Ma Devine Canyon Tuff is cut and ponded against a northwest-striking fault (Johnson, 1995). A variety of observations indicate that extension after eruption of the Steens Basalt but prior to the deposition of the Devine Canyon Tuff occurred to the northeast of the Brothers fault zone and to the to the north-northwest, on the footwall, of the Steens Mountain range-front fault (the Crane Basin, Day 3, morning). Thus, the Steens Mountain fault and faults formed in the footwall block to the north-northwest delineate the western margin of the Basin and Range prior to ca. 10 Ma.

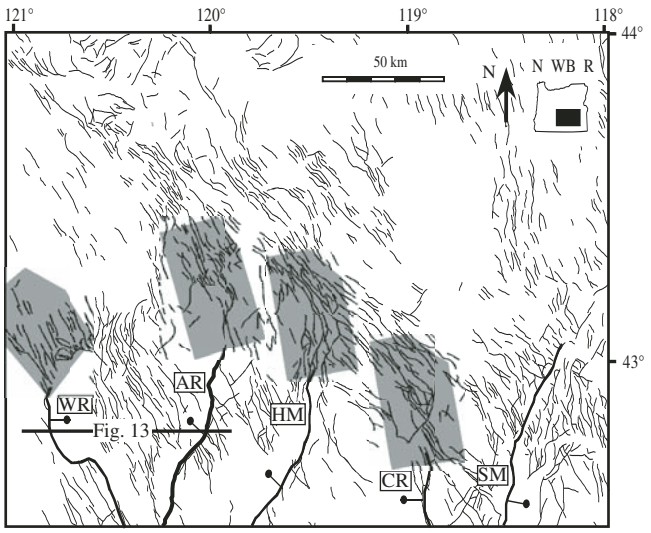

Figure 6. Faults in the northwest Basin and Range and Brothers fault zone. From Trench (2008), using data in Walker and MacLeod (1991). Shaded boxes indicate zones of transition at the tips of large-displacement (>150 m) Basin and Range faults (thick lines). Small-displacement faults are thin lines. WR—Winter Ridge; AR—Abert Rim; HM—Hart Mountain; CR—Catlow Rim; SM—Steens Mountain.

Deformation jumped to the west after ca. 10 Ma. By 7 Ma, extension rates in the Crane Basin had diminished and deformation shifted west to form the Harney Basin (Day 3). Structural and stratigraphic relations indicate that northwest-striking faults associated with the Abert Rim fault system were active between 8.7 and 7.6 Ma (Scarberry et al., 2009). Northward propagation of the Abert Rim fault system, in part as the result of linking of individual segments, occurred after 7.6 Ma. Structural relations and partial restorations of faults forming the Hart Mountain system indicate that this fault grew into the Brothers fault zone, which had a down-to-the-northeast fabric that was likely established by 7 Ma (Day 2, Alec Butte stop). Rate of extension on these two fault systems varies from ~0.1 mm/yr between ca. 7 and 5.7 Ma to ~0.01 mm/yr after ca. 5.7 Ma (Trench, 2008). The Abert Rim fault system displays similarly variable extension rate, although the period of relatively higher rate (~0.1 mm/yr) occurs earlier (7.6–7.0 Ma) than is inferred for the Hart Mountain fault system to the east (Scarberry et al., 2009). After ca. 7 Ma, extension rate dropped to 0.01 mm/yr.

DAY 1. QUATERNARY MAGMATISM IN THE CASCADE RANGE—BASIN AND RANGE TRANSITION, NEWBERRY VOLCANO AREA (FIGURE 7)

Newberry Volcano, named for Dr. John Strong Newberry, a member of the 1855 Topographic Corps Expedition, is a large shield volcano situated ~60 km east of the Cascade crest, 30 km southeast of Bend, Oregon (Fig. 8). The caldera rim reaches to an altitude of 2434 m at the summit of Paulina Peak. The volcanic edifice was built from eruptions over the past 0.5 m.y., the most recent of which is the ~1300-year-old Big Obsidian Flow, erupted within the summit caldera (Jensen, 2006) (Fig. 9). The caldera formed ~80,000 years ago during an eruption of a compositionally zoned rhyolitic to andesitic ash-flow tuff (Jensen et al., 2009). The volcano's summit area and a rift system that extends to the northwest were designated as a National Volcanic Monument by the U.S. Department of Agriculture Forest Service in 1990. Additional

information on Newberry is available in the field guide for the pre-meeting field trip concentrating on Newberry (Jensen et al., 2009), which builds on a previous guidebook (Jensen, 2006) and ongoing work by J.M. Donnelly-Nolan, R.A. Jensen, and D.W. Ramsey.

Newberry Volcano has been constructed by lava flows ranging from basalt to rhyolite, with a concentration of activity toward these two end-member compositions. Newberry has erupted numerous primitive basalt flows (Table 2; Fig. 10). These HAOT lavas are nearly aphyric, equigranular basalt with an intersertal texture. Many of the lavas are vesicular and display a well-developed diktytaxitic texture. Geochemically, these lavas can be divided into two groups. The first is similar in composition to the HAOT distributed widely across the High Lava Plains. These basalts are characterized by relatively smooth normalized incompatible element abundances showing only slight relative enrichment in the more incompatible elements (Table 2, col. 2; Fig. 10). The other type of basalt shows a stronger calc-alkaline major element signature (slightly higher SiO_2 and K_2O, and lower FeO and TiO_2)

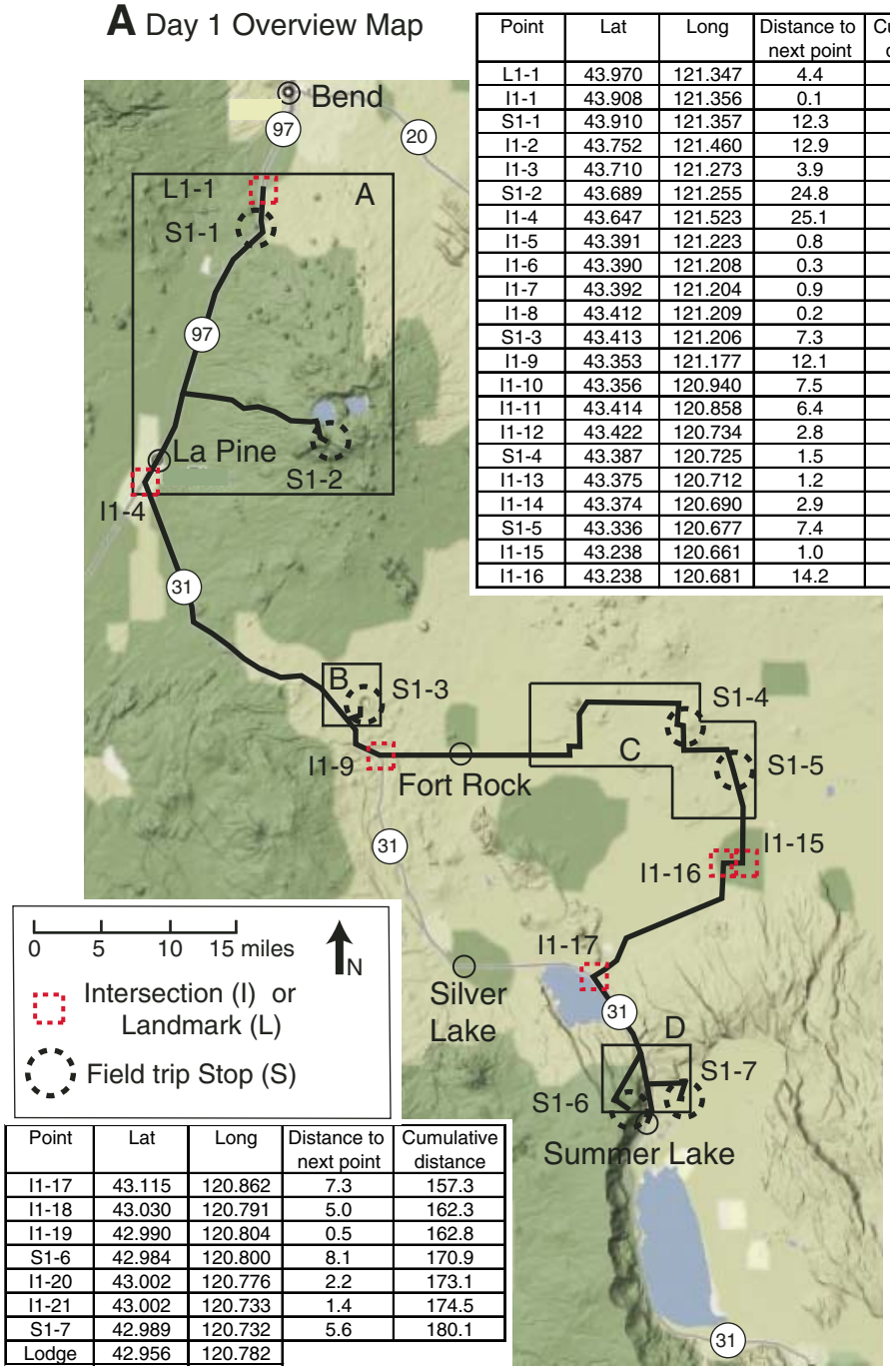

Point	Lat	Long	Distance to next point	Cumulative distance
L1-1	43.970	121.347	4.4	4.4
I1-1	43.908	121.356	0.1	4.5
S1-1	43.910	121.357	12.3	16.8
I1-2	43.752	121.460	12.9	29.7
I1-3	43.710	121.273	3.9	33.6
S1-2	43.689	121.255	24.8	58.4
I1-4	43.647	121.523	25.1	83.5
I1-5	43.391	121.223	0.8	84.3
I1-6	43.390	121.208	0.3	84.6
I1-7	43.392	121.204	0.9	85.5
I1-8	43.412	121.209	0.2	85.7
S1-3	43.413	121.206	7.3	93.0
I1-9	43.353	121.177	12.1	105.1
I1-10	43.356	120.940	7.5	112.6
I1-11	43.414	120.858	6.4	119.0
I1-12	43.422	120.734	2.8	121.8
S1-4	43.387	120.725	1.5	123.3
I1-13	43.375	120.712	1.2	124.5
I1-14	43.374	120.690	2.9	127.4
S1-5	43.336	120.677	7.4	134.8
I1-15	43.238	120.661	1.0	135.8
I1-16	43.238	120.681	14.2	150.0

Point	Lat	Long	Distance to next point	Cumulative distance
I1-17	43.115	120.862	7.3	157.3
I1-18	43.030	120.791	5.0	162.3
I1-19	42.990	120.804	0.5	162.8
S1-6	42.984	120.800	8.1	170.9
I1-20	43.002	120.776	2.2	173.1
I1-21	43.002	120.733	1.4	174.5
S1-7	42.989	120.732	5.6	180.1
Lodge	42.956	120.782		

Figure 7 (*continued on following page*). (A) Overview of Day 1 route with stop, intersection, and landmark coordinates. (B–E) Detailed maps of each stop. Stops are indicated with the letter S followed by the day and stop number. Key intersections (I) and prominent landmarks (L) are indicated. Distances are in miles. Note that the Ana River active fault stop S1–7 will visit a newly exposed trench at intersection I1–21. Figures 14–16 are from the point marked S-7 and will be visited if time and access permit.

compared to the HAOT (Table 2, col. 3; Fig. 10). The calc-alkaline lavas show dramatically different normalized incompatible element patterns compared to the HAOT, with both strong enrichment in the more highly incompatible elements and the development of strong relative deficiencies in high-field-strength elements like Nb and Ta and enrichments of fluid-mobile elements like Ba and Sr (Fig. 10). The two compositional types are distinguished by small but reproducible differences in isotopic composition, with the calc-alkaline lavas having slightly higher $^{87}Sr/^{86}Sr$ and $^{187}Os/^{188}Os$, and lower $^{143}Nd/^{144}Nd$ than the HAOT. The range in isotopic composition, however, is small, with the HAOT extending to $^{87}Sr/^{86}Sr$ as low as 0.70322 and the calc-alkaline lavas to as high as 0.70382. The Big Obsidian Flow has a $^{87}Sr/^{86}Sr$ of 0.70364 (Table 2, col. 1), testifying to the limited range of isotopic composition of Newberry lavas despite their wide compositional range.

Driving Instructions

Details of our visit to Newberry Volcano depend on weather-related access. If the autumn snows have not yet arrived, we will make one stop at the Paulina Peak overlook (Stop 1-2), Newberry's summit. If this is not feasible, then two stops will be made on the flanks of the volcano, one at Lava Butte and the second at Hole in the Ground. Note that on the figures and in the tables related to the driving instructions the letter (S) indicates a Stop, (I) indicates a critical intersection, and (L) denotes prominent landmarks

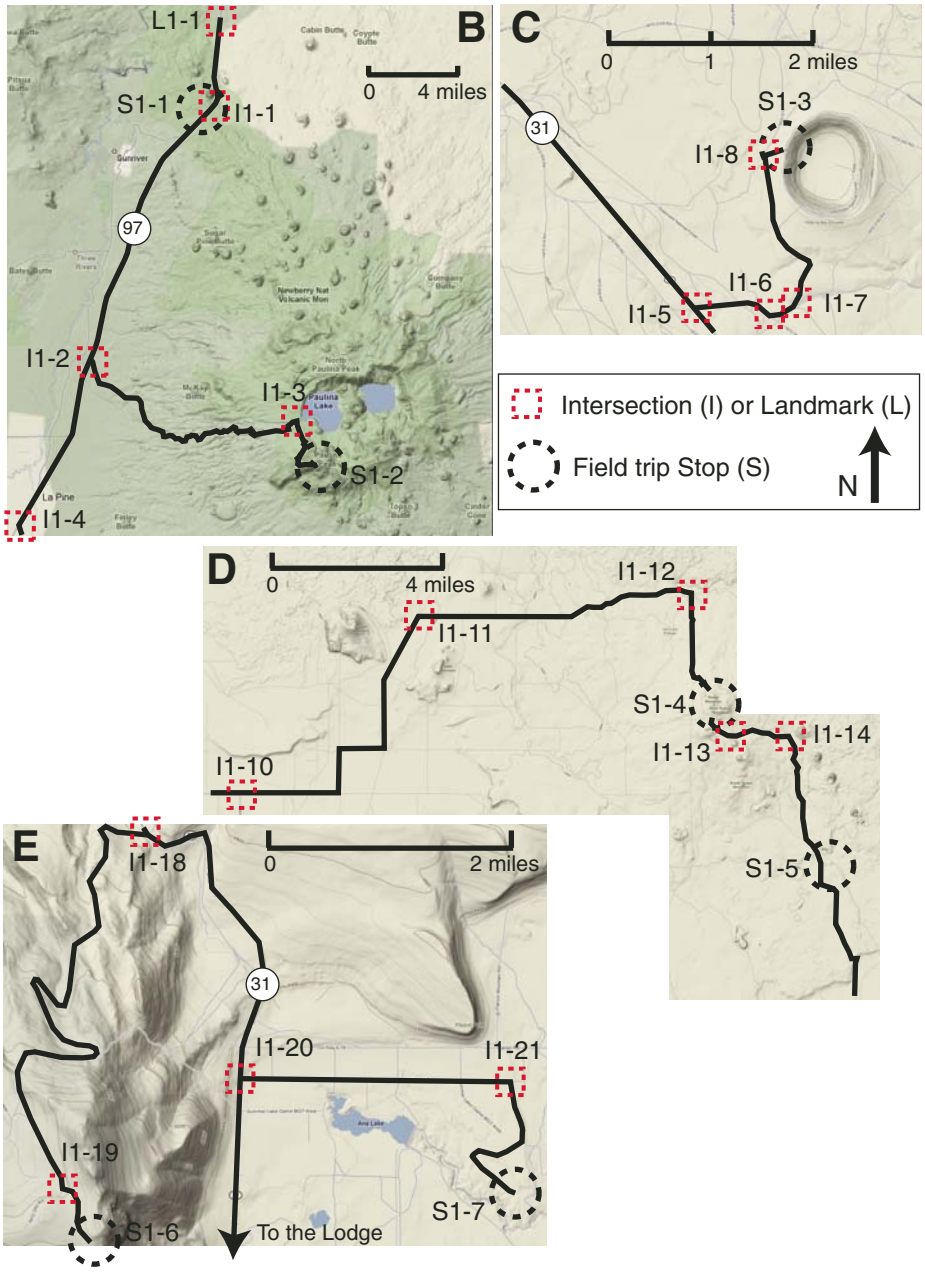

Figure 7 (*continued*).

Travel south from Bend on U.S. Highway 97. Continue 4.4 miles beyond the entrance to the High Desert Museum (L1-1). Turn right (I1-1) into the Lava Lands Visitor Center for stop 1 at Lava Butte (S1-1). The lookout tower on top of Lava Butte, if open, provides the best viewpoint.

Stop 1-1. Lava Butte (43.910°N, 121.357°W)

Lava Butte is the northernmost vent along a Holocene fissure that extends over 30 km southeast to Newberry caldera. The Lava Butte eruption, which occurred ~7000 years ago (MacLeod et al., 1975), began as a 2.4-km-long fissure with eruptive activity eventually becoming concentrated at the site of Lava Butte (Jensen et al., 2009). Lava Butte itself is a 150-m-high cinder cone, but the eruption's products include spatter ramparts and lavas flows that cover a total of 23 km^2. The flows erupted from various vents along this fissure range considerably in composition, with SiO_2 from 51.3 to 58.4 wt%, whereas the flows from Lava Butte show a more restricted range, from 55.3 to 56.2 wt% (Jensen et al., 2009).

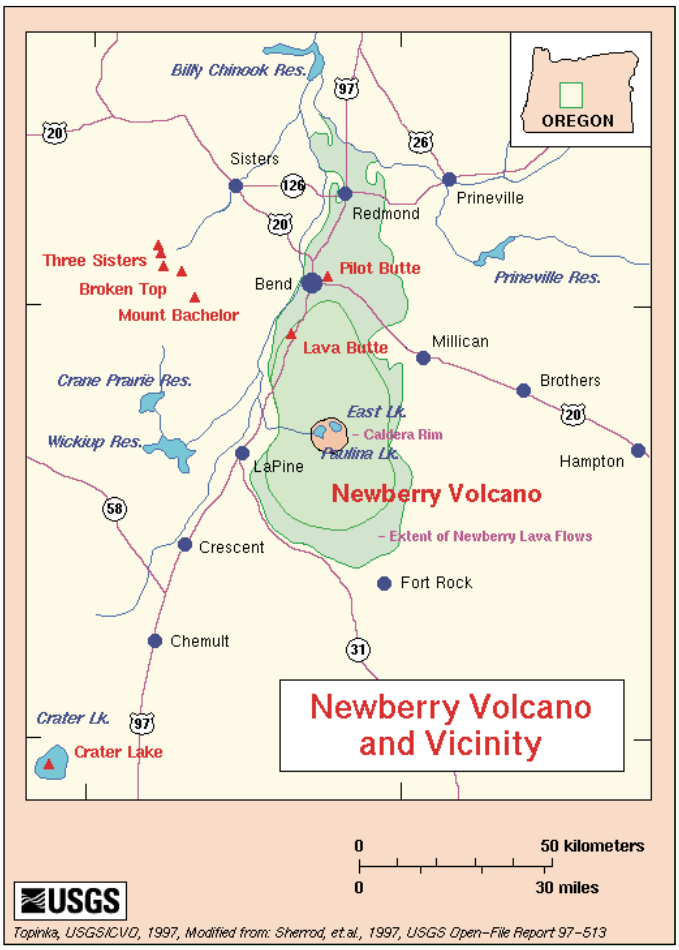

Figure 8 (Stop 1-2). Regional geographic setting of Newberry Volcano and vicinity. Shading indicates extent of Newberry's volcanic edifice and associated lava flows. From Sherrod et al. (1997).

Besides the opportunity to examine features of this young basaltic andesite eruption, this location allows a broad view of the topographic variation and nature of volcanism seen sequentially eastward from the Cascade Range, across Newberry Volcano, and onto the High Lava Plains. In the distance to the west of Lava Butte, the largely intermediate composition stratovolcanoes of the High Cascades, notably the Three Sisters complex and Mount Bachelor, are visible. Mount Bachelor, the culminating vent in a lengthy volcanic chain to its south, is chiefly basaltic andesite. Looking to the southeast, the gentle slopes of the broad Newberry shield volcano are dotted by numerous small eruptive centers. More evolved lava flows, particularly the intermediate to silicic components of Newberry volcanism, are concentrated toward the caldera, in the center of the Newberry shield.

Driving Instructions

After leaving Lava Butte, drive south on U.S. Highway 97 ~12.2 miles and turn left (east) onto County Route 21, the Paulina Lake Road (I1-2), paved. Drive ~12.9 miles to the rim of the caldera, and then turn right (south) (I1-3) along Forest Service Road 500, the Paulina Peak road (gravel). Continue 3.9 miles to the Paulina Peak overlook (S1-2).

Stop 1-2. Paulina Peak (43.689°N, 121.255°W)

Paulina Peak, at 2434 m, provides an excellent vista into Newberry caldera, down the flanks of the shield, and a wide view of the changing topography from the Cascades to the west, east into the High Lava Plains. As described in (Jensen, 2006), the parking lot atop Paulina Peak is built on top of the drilling pad for Occidental

Figure 9 (Stop 1-2). View northeast across Newberry caldera from Paulina Peak. The barren flow in center is the Big Obsidian Flow, which erupted from near the south wall of the caldera. The Big Obsidian Flow is one of several intracaldera eruptive events active after formation of the caldera ~80,000 years ago.

TABLE 2. MAJOR ELEMENT AND ISOTOPIC COMPOSITION OF SELECT NEWBERRY LAVAS IN COMPARISON TO HAOT FROM FURTHER EAST ON THE HIGH LAVA PLAINS (HLP)

Location:	Newberry	Newberry	Newberry	HLP	HLP
Unit:	Big Obsidian Flow	Red Near	Luna Butte	Diamond Crater	Virginia Valley
SiO_2	72.81	49.10	50.20	48.01	48.35
TiO_2	0.23	1.32	1.17	1.33	0.94
Al_2O_3	14.02	17.62	16.10	17.71	17.45
FeO*	2.05	9.39	7.86	10.26	10.04
MnO	0.06	0.16	0.14	0.18	0.18
MgO	0.19	8.53	9.40	8.57	9.23
CaO	0.85	11.26	10.84	10.87	11.44
Na_2O	5.23	2.96	2.98	2.95	2.59
K_2O	4.02	0.27	1.12	0.40	0.24
P_2O_5	0.03	0.16	0.50	0.22	0.12
Sum	99.49	100.76	100.31	100.49	100.57
Loss on ignition (%)	0.24	–0.45	0.00	–0.62	–0.35
$^{87}Sr/^{86}Sr$	0.703639	0.703168	0.703816	0.703968	0.704763
$^{143}Nd/^{144}Nd$	0.512895	0.513032	0.512918	0.512865	
$^{206}Pb/^{204}Pb$		18.952	18.969	18.862	18.886
$^{207}Pb/^{204}Pb$		15.602	15.608	15.580	15.616
$^{208}Pb/^{204}Pb$		38.522	38.643	38.567	38.800

Geothermal's drill site NC72-03. The hole reached a depth of 1370 m and encountered a temperature of 155 °C in the bottom of the hole. The upper 550 m of the hole sampled numerous near-vent lava types while the next 150 m was mostly in silicic lava flows. The lower 670 m of the hole penetrated basaltic andesite (Arestad et al., 1988). From this vantage point, the caldera wall and numerous intracaldera intrusions and lava flows are well displayed. The most obvious is the Big Obsidian Flow (Fig. 9), which erupted from near the south wall of the caldera and flowed north nearly to the caldera's center. Separating Paulina and East Lakes in the caldera are Little Crater, a basaltic tuff cone; the Central Pumice Cone; and the Interlake Obsidian Flow (MacLeod et al., 1995). A prominent stratigraphic marker in this area is the 7700-year-old fallout ash from the cataclysmic eruption of Mount Mazama, nearly 100 km to the southwest (c.f., Bacon, 2008); it mantles all older deposits on Newberry Volcano. Several of the intrusive and flow units within the caldera postdate the Mazama ash deposit, including several silicic eruptive centers ~7100 years in age, the 3500-yr-old East Lake Obsidian Flows, and the 1250–1300-yr-old Big Obsidian Flow.

Looking from Paulina Peak down the north and south flanks of the Newberry shield, the numerous cinder and spatter cones delineating young eruptive centers on the flanks of Newberry can be observed. Whereas the silicic volcanic activity at Newberry has been clustered near the caldera, eruptions of basalt to basaltic andesite occurred from numerous localities along the flanks of the shield. On the northern margin, several basalt flows extend from Newberry to the north beneath Bend and Redmond (Fig. 8). One of the more northerly eruptive centers is that of Lava Butte (Stop 1-1). To the south, the flows of Newberry reached nearly to Fort Rock Lake. Fort Rock Lake, one of several large Pleistocene lakes in this area filled the Christmas Valley to the south of Newberry to a depth of as much as 45 m. Eruptive centers that were active when the lake was extant formed a variety of phreatomagmatic maars, such as that seen at Hole in the Ground (Stop 1-3; Fig. 7), and large tuff rings like that forming Fort Rock itself.

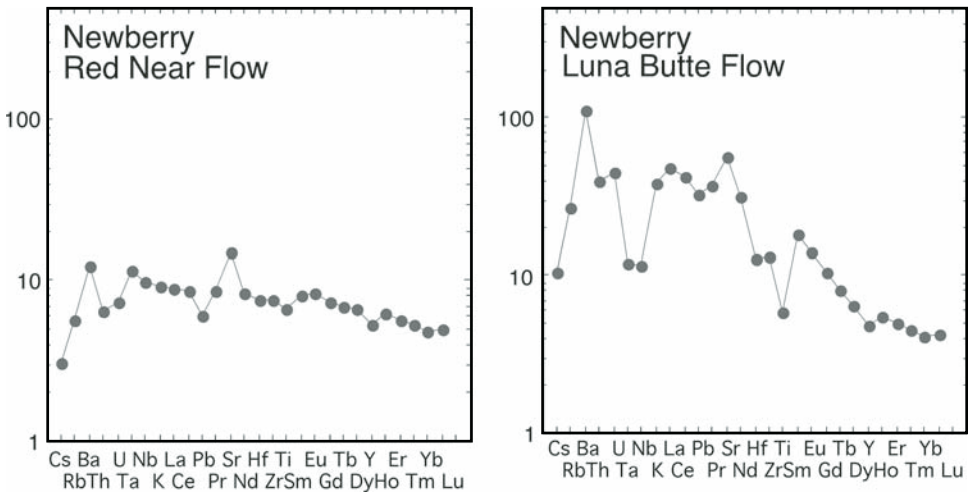

Figure 10 (Stop 1-2). Incompatible element abundances of two Newberry Volcano basalts normalized to the bulk silicate earth values of McDonough and Sun (1995). Major element analyses in Table 2.

Driving Instructions

Return to Highway 97 (I1-2) and continue south for 8.0 miles, passing through the town of La Pine while skirting the flows that issued from Newberry Volcano. Turn left (east) onto Oregon Highway 31 (I1-4) continuing along the southern reaches of the Newberry lavas. Continue 25.1 miles and turn onto Forest Service Road 3145 (I1-5), unpaved. Unpaved roads in this area may be impassable when saturated or in the springtime. Drive 0.8 miles and take a left (I1-6). Continue another 0.3 miles and veer left (I1-7) onto Forest Service Road 3130. Continue 0.9 miles to the intersection of Forest Service Road 200 (I1-8) and turn right (east). Drive 0.2 miles to the Hole-in-the-Ground parking lot (S1-3).

Stop 1-3. Hole-in-the-Ground (43.413°N, 121.206°W)

As described by (Jensen, 2006), Hole-in-the-Ground is a maar formed when Newberry magmas entered the water-saturated sediment of the Fort Rock basin, perhaps as early as 50,000–100,000 years ago. The magma may have been rising along a fault that is exposed in the crater walls. Hole-in-the-Ground is one of many expressions of phreatomagmatic activity in this area. The most picturesque example is Fort Rock, which can be seen 11 km to the east-southeast. Fort Rock is a 1370-m-diameter, 60-m-high tuff ring formed in deeper water of the Fort Rock basin. Highway 31 passes near Fort Rock en route to subsequent stops.

Upslope to the north is an excellent view of the abundant young cinder-cone-forming eruptions scattered widely across the southern and southeastern flanks of Newberry Volcano.

Driving Instructions

(This Green Mountain stop is weather and time dependent.)

Return to Oregon Highway 31 (I1-5), turn left (south) and travel 5.1 miles and turn left (east) onto County Route 5-10, Fort Rock Road (I1-9), paved. Continue 12.1 miles, passing through the small town of Fort Rock, to the intersection of Fort Rock Road and Derricks Cave Road, County Route 5-12 (I1-10). Continue straight (east) on Derricks Cave Road for 7.5 miles (the Fort Rock Road turns to the south). Stay on the paved road though a series of a left, right, and left again 90° turns and note Cougar Mountain, a coulee-encircled 4.34 Ma (Fig. 4) monogenetic rhyolite dome, complete with glassy carapace, on the left. At the intersection of County Route 5-12B, the Sink Road (I1-11), turn right (east). Drive 6.4 miles to the intersection with Bureau of Land Management (BLM) Road 6109-C (I1-12) and turn right (south). Continue 2.8 miles to Green Mountain (S1-4).

Stop 1-4. Green Mountain Lookout Overview (43.387°N, 120.725°W)

If visibility is poor, this stop is to be omitted. Green Mountain is a basalt shield that fed the lava flow at the Crack-in-the-Ground, ~740,000 years ago (Jordan et al., 2004; Jordan et al., 2002). The fire lookout at this location offers a panoramic overview of the western High Lava Plains and the northwestern Basin and Range. To the north, Hampton Butte (Stop 3-4) is faintly visible on the northern margin of the High Lava Plains (Fig. 11). To the east are the volcanic buttes of the central High Lava Plains: Glass Buttes (two lumps at N70°E); Round Butte (N80°E); Paiute Butte (pointed butte at N82°E); Wagontire Mountain (S87°E); Horsehead Mountain (S74°E); Elk Mountain (S73°E); Little Juniper Mountain (S70°E); and Horse Mountain (S61°E). To the south is Christmas Valley with Table Rock, and in the background is Winter Ridge (a Basin and Range escarpment). To the southwest is Fort Rock, a palagonitized tuff ring.

From this location we have an excellent view of the "East lava field" to the north. The lava field was erupted from the summit of the Lava Mountain shield, which is marked by a 1.6-km-long series of craters aligned N20°W. Obscured from our view by the east summit of Green Mountain is the Four Craters lava field, with its eponymous four northwest-aligned vents. Like the East lava field, the Four Craters field is post-Mazama ʻaʻā basalt. It is compositionally identical to the East lava field, and the northwest trend of the four-craters alignment projects nearly to the summit

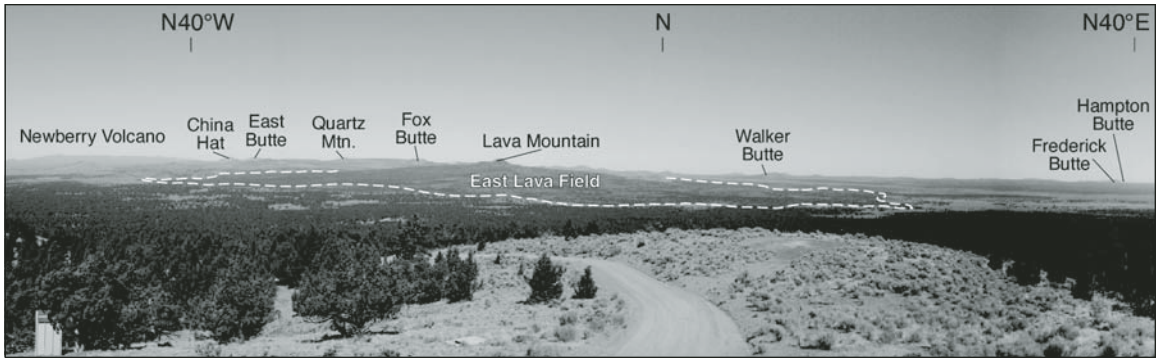

Figure 11 (Stop 1-4). Panoramic view north across High Lava Plains from summit of Green Mountain.

of Lava Mountain. These relations suggest that the Four Craters and East lava fields are related. We will get a closer look at the Four Craters lava at the next stop.

Lunch at the campground below the lookout.

Driving Instructions

Continue to the southeast, after 1.5 miles, bear right at the fork in road (I1-13). The left fork goes to Green Mountain East. As the road approaches the margin of the Four Craters lava, note distinct ‘a‘ā flow morphology. Drive 1.2 miles and turn right (south) at the flow onto BLM Road 6109, Lava Road (I1-14) then continue on 2.9 miles to Crack-in-the-Ground (S1-5). There is a small parking area on the left.

Stop 1-5. Volcanism and Faulting: Crack-in-the-Ground (43.336°N, 120.677°W)

This locality features a great northwest-striking crack, Crack-in-the-Ground, developed in the Green Mountain lava (740 ± 59 ka, Jordan et al., 2004, Fig. 10). The crack coincides with a Quaternary normal-fault trace that extends beyond the crack to the north and the south, strong evidence for a tectonic interpretation (Peterson and Groh, 1964; Pezzopane and Weldon, 1993). The crack penetrates more than one lava flow, further evidence for a tectonic rather than volcanic origin. There are ~10 m of vertical displacement between rocks southwest (high) and northeast (low) of the crack. The crack has developed in what is essentially the upper hinge of a monocline generated by displacement on a steep normal fault below. Similar features are described in transverse fault zones in Iceland (e.g., Gudmundsson et al., 1993).

From the parking area, head east on the marked trail to Crack-in-the-Ground. At the crack, go right (southeast) and enter the crack. In this segment, the crack is deep and narrow, which aids in the visual matching or surface irregularities on opposite sides of the crack match (pure normal separation). Now reverse direction and proceed northwest. View the crack from within and also from the east side to appreciate the generally monoclinal structure that has formed here. In the crack, look for places where more than one flow has been cracked. Follow the crack to where the Four Craters lava flowed into the crack. Continue along the southwest margin of the Four Craters lava. Pezzopane and Weldon (1993) suggest that the Four Craters lava has itself been cracked (though to a lesser degree than the Green Mountain lava), indicating Holocene displacement on this structure (Fig. 12). Evidence for development of the crack in the younger lava is ambiguous.

Driving Instructions

Return to vehicles and continue south on Lava Road, which becomes Crack-in-the-Ground Road, to Christmas Valley Road (I1-15), turn right and go west 1.0 miles. At Christmas Tree Lane (I1-16), turn left, which becomes County Route 5-14F, Old Lake Road (may also be labeled Wagontire Road). Continue 14.2 miles southwest to the intersection with Highway 31 (I1-17). Turn left (southeast) and drive 7.3 miles to the intersection with Forest Road 290 (I1-18). Turn to right (southwest) and proceed 5.0 miles uphill to the intersection with an unnamed forest road (I1-19) and turn left. Continue ~0.5 miles to view point (S1-6). Parking and space to turn around is limited.

Stop 1-6. Active tectonics of the Basin and Range Overview from Winter Ridge (42.984°N, 120.800°W)

At this view stop on Winter Ridge, an overview of the structure and active tectonics of the northwestern Basin and Range extensional province will be presented. The stop is in the footwall of the Winter Ridge fault system and the hanging wall half graben containing Summer Lake can be seen to the southeast. To the east, north-northwest–trending faults seen to the north of the north shore of Summer Lake include the Ana River fault, which will be visited at Stop 1-7.

After the Klamath graben along the western edge of the Basin and Range extensional province in Oregon, the north-trending Winter Ridge fault system defines the first prominent extensional escarpment (Badger and Watters, 2004; Pezzopane and Weldon, 1993). An east-dipping fault system composed of numerous individual fault strands defines the Winter Ridge fault system, individual segments of which are partly obscured by prolific landslides along the base of Winter Ridge (Badger and Watters, 2004). Like Lake Abert to the east, Summer Lake sits on the hanging wall adjacent to the rim-bounding fault system (Fig. 13). Topographic relief across the north end of the Winter Ridge fault system diminishes to the north as the fault system terminates in an array of northwest-striking faults (Fig. 6). This same geometric configuration occurs at the northern ends of the Abert Rim and

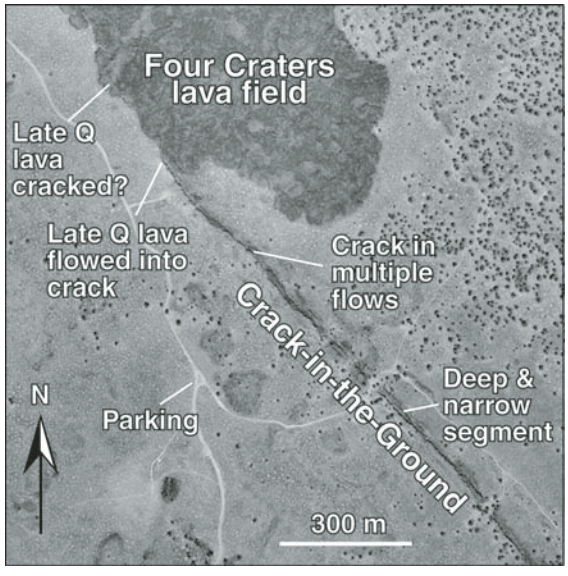

Figure 12 (Stop 1-5). Aerial photo of Crack-in-the-Ground.

Hart Mountain fault systems, to the east (Scarberry et al., 2009; Trench, 2008). Unlike those two fault systems, where the transition from north-northeast–striking faults to northwest-striking faults occurs along the southwestern edge of the Brothers fault zone, the termination of the Winter Ridge fault system into the northwest-striking faults occurs south of the Brothers fault zone. The Ana River fault is one of the north-northwest–striking faults to the north of the Winter Ridge fault system, and both faults have evidence of Holocene activity (Badger and Watters, 2004; Langridge et al., 2001; Pezzopane and Weldon, 1993).

Driving Instructions

Return to the Highway 31 intersection (I1-19). Turn southeast (right) on Highway 31 and proceed 2.6 miles to intersection with Game Management Boundary Road which may be labeled Lakeview Road (I1-20). This intersection is 0.2 miles south of the paved Carlon Road–Highway 31 intersection. Turn left and proceed east 2.2 miles to intersection (I1-21). Proceed south 1.4 miles to fishponds of Desert Springs Trout Farm (S1-7). Note that this is private land, and permission must be obtained to visit the site.

Stop 1-7. Active tectonics of the Basin and Range–Ana River fault, Summer Lake (42.989°N, 120.732°W)

A Pleistocene pluvial lake, Lake Chewaucan, occupied the structural low bound by the Winter Ridge to the west and Abert Rim to the east (Allison, 1982). Shorelines of Lake Chewaucan are draped around the lower slopes of hills within the Chewaucan basin and are visible as high as ~4500 ft (Pezzopane, 2001). In general, both the Ana River and Winter Ridge faults cut these shorelines, although relations between fault scarps, landslide deposits, and pluvial lake shorelines indicate a complex sequence of faulting on individual fault segments, landsliding, and pluvial lake recession (Badger and Watters, 2004; Langridge et al., 2001; Pezzopane and Weldon, 1993). At this stop, we will examine paleoseismic evidence for earthquakes on the Ana River fault from excavations across a scarp located where the southern end of the Ana River fault crosses the Ana River on the grounds of the Desert Springs Trout Farm. Note that this is private land and permission must be obtained to visit the site. What follows is a summary of published work by Rob Langridge and Silvio Pezzopane and is based on data collected in a set of trenches on the south side of the Ana River (Langridge et al., 2001; Pezzopane and Weldon, 1993) (Figs. 14, 15, and 16). A recently excavated trench to the north of the site will be visited.

An ~2–4-m-high scarp characterizes the fault trace at the Trout Farm (Langridge et al., 2001). The fault cannot be traced into the Summer Lake basin because the scarp has been eroded by a ca. 2 ka Summer Lake shoreline, which constrains the age of the last surface rupturing earthquake to prior to 2 ka. Langridge, Pezzopane, and Weldon have excavated trenches on both the north and south banks of the Ana River, and the earthquake chronology is a composite of relations within those excavations. Representative trench logs demonstrate one type of structural evidence for surface rupture (Fig. 15). Evidence of surface rupture was revealed by excavations to the south of the river (the "River" trenches, Fig. 16) and at Kippel Point to the north. These data, when combined with ages of key tephra beds, suggest surface-rupturing earthquakes between 2160 and 7600 yr B.P., 12–14 ka B.P., 29.1 ± 2 ka, 49 ± 5 ka, 70 ± 6 ka, and 81 ± 6 ka (Fig. 14). Offsets and scarp height at the Kippel site suggest fault slip rate is 0.17–0.23 mm/yr, the low rate of which is consistent with the slip rates inferred for the majority of the other principal north-trending extensional faults in south eastern Oregon (Pezzopane and Weldon, 1993).

Driving Instructions

Return to Highway 31 and proceed south ~2 miles to Summer Lake and overnight at Summer Lake Lodge.

DAY 2, MORNING. PRE–BASIN AND RANGE MAGMATISM AND TIMING OF ONSET OF EXTENSION ABERT RIM AND COLEMAN HILLS (FIGURE 17)

The morning will be spent examining Lower Miocene rocks exposed along the Abert Rim fault at Coleman Hills and Grays Butte.

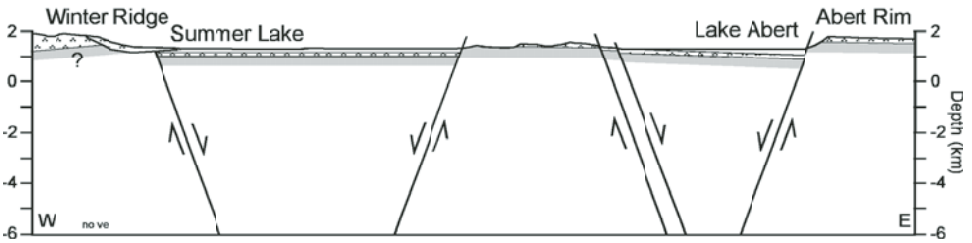

Figure 13 (Stop 1-6). Cross section across the compound graben between the Winter Ridge and Abert Rim range-front fault systems. Dark shading represents the Steens Basalt; stratigraphic units above the Steens Basalt are undifferentiated sedimentary and volcanic deposits, which have partly filled basins formed by the two fault systems. Thicknesses from Scarberry et al. (2009). Whether Steens Basalt underlies Winter Ridge is uncertain.

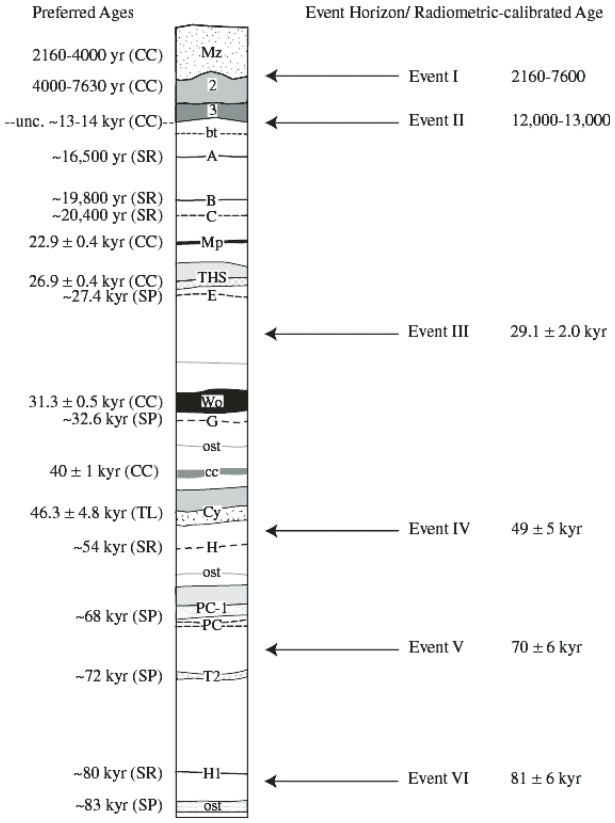

Figure 14 (Stop 1-7). North Summer Lake composite stratigraphic column showing tephra beds (dated horizons) and paleoseismic event ages, which are constrained by tephra ages, calendar calibrated radiocarbon ages (CC), sedimentation rate (SR) estimates, stratigraphic position (SP), and thermoluminescence (TL). Abbreviations in the stratigraphic column: Mz is Mazama ash-rich dune deposit; 2 and 3 are post-lake highstand subaerial units; bt is black tephra; A, B, C, E, G, H, and H1 are tephras recognized throughout the Lake Chewaucan basin (Davis, 1985); Mp is pumice of Castle Rock (an earlier Mount Mazama eruption); THS is Trego Hot Spring ash; Wo is Wono ash; ost are ostracod layers; cc are calcium carbonate layers; Cy is Mount St Helens Cy (y of the C series); and PC and PC-1 are Pumice Castle set. Illustration from Langridge et al. (2001).

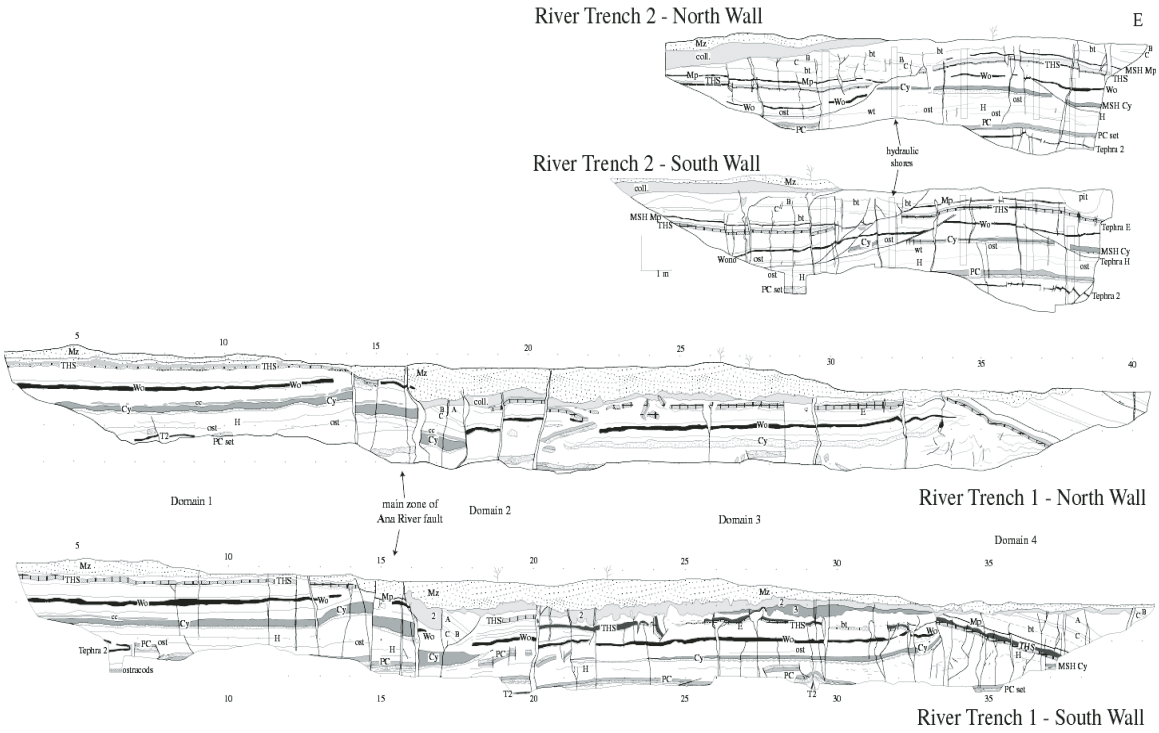

Figure 15 (Stop 1-7). Interpreted logs of the north and south walls of two trenches excavated across the Ana River fault on the south side of the river from the trout farm. The east (right) ends of the trenches overlap the same structures. The two trenches were excavated ~2 m apart.

Background

The Cenozoic tectonic and magmatic evolution of western North America has bred an extensive and controversial literature debating diverse tectonic models to account for distinct tectonomagmatic episodes. The geologic record in the High Lava Plains and northwest Basin and Range is best examined in terms of three distinct phases (1) Early Miocene, >20 Ma, dominantly intermediate composition volcanism, (2) Middle Miocene, ca. 17–14 Ma fundamentally bimodal volcanism highlighted by the Steens Basalt event, which flooded the region beginning at ca. 16.6 Ma, and (3) Late Miocene, post–10 Ma volcanism that is characterized by widespread basalt eruptions and age-progressive rhyolite eruptions of the High Lava Plains.

The geologic history prior to the middle Miocene is difficult to unravel because exposures are covered by the 16.6–15.3 Ma flood basalts associated with Steens Mountain volcanism (Brueseke et al., 2007; Hooper et al., 2002) and by post–10 Ma bimodal basalt-rhyolite volcanism of the High Lava Plains (Johnson, 1995; Johnson et al., 1998). Eocene to Lower Miocene volcanic rocks are widely exposed north of the High Lava Plains, within the John Day Basin. They presumably underlie the High Lava Plains, since ~30-m.y.-old Hampton Butte (Iademarco, 2009) lies at the northern edge of the High Lava Plains (Day 3 stop S3-4) and rocks emplaced between 26 and 20 Ma crop out in fault scarps in the northwest Basin and Range (Langer, 1991; Mathis, 1993; Scarberry et al., 2009). The upper Oligocene and lower Miocene volcanic rocks were emplaced chiefly as trachyandesite composite volcanoes with satellite vents and domes of trachyte and rhyolite, but they range from basaltic andesite strombolian volcanic rocks to rhyolite ignimbrites and even pantellerite (Mathis, 1993).

A paucity of radiometric ages for the interval between 19 and 17 Ma implies a brief magmatic hiatus during that time. Volcanism in the High Lava Plains–northwest Basin and Range region volcanism resumed ca. 16.6 Ma. The most obvious marker of this change is the emplacement of dikes and the eruption of massive flood basalts along a ~700-km-long north-trending zone along the western margin of Precambrian North America, including the Northern Nevada Rift (Zoback et al., 1994), dikes of the

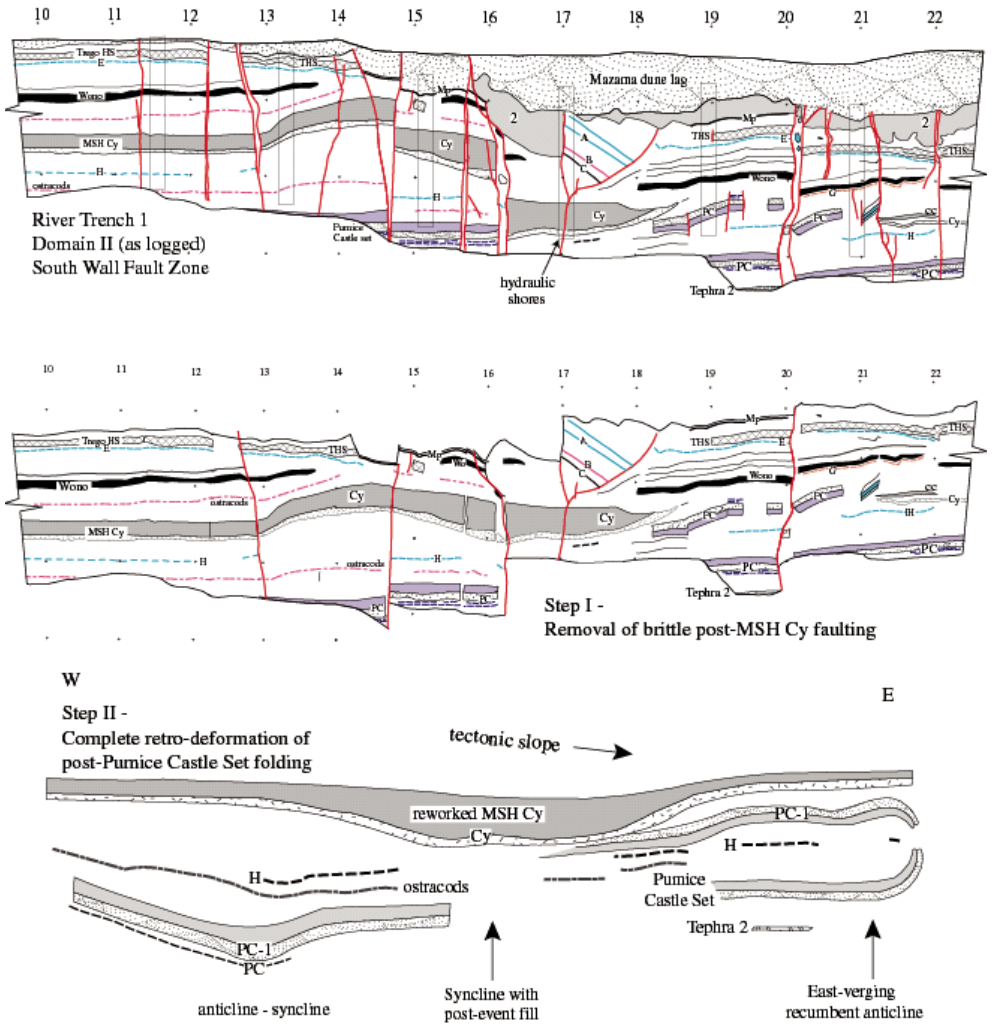

Figure 16 (Stop 1-7). A progressive reconstruction of the River trench South Wall trench logs constrains the timing of paleoearthquakes. Note that age constraints on surface-rupturing events are constrained by the Mazama Pumice, Pumice of Castle Rock, and the Mount St. Helens (MSH) Cy tephra.

Steens Basalt at Steens Mountain (Brueseke et al., 2007; Camp et al., 2003; Carlson and Hart, 1987; Hooper et al., 2002) and the dike swarms of the Columbia River Basalt Group (CRBG) farther north (e.g., Hooper et al., 1997). In the Oregon-Nevada-Idaho border and northwest Basin and Range regions, the flood basalt volcanism was accompanied by large volume rhyolitic activity at localities such as McDermitt (Conrad, 1984; Rytuba and McKee, 1984) and Virgin Valley (Castor and Henry, 2000), and at other volcanic fields around the margins of Owyhee Plateau (Brueseke and Hart, 2008; Ekren et al., 1982). Based on its plate-motion-direction projection from the hotspot track along the central-eastern Snake River Plain, the McDermitt area often is identified as the impact point of the Yellowstone mantle plume (Camp et al., 2003; Hooper et al., 1997; Suppe et al., 1975). However, predominantly bimodal volcanism from ca. 17–14 Ma was widely scattered across southeast Oregon and northern Nevada (Brueseke and Hart, 2008). During the waning stages of the mid-Miocene bimodal volcanic period, High Lava Plains region volcanism became more localized such that, by ca. 11–12 Ma, activity was focused toward the area that now forms the western margin of the Owyhee Plateau (Hart et al., 1984; Russell et al., 1988; Shoemaker and Hart, 2001).

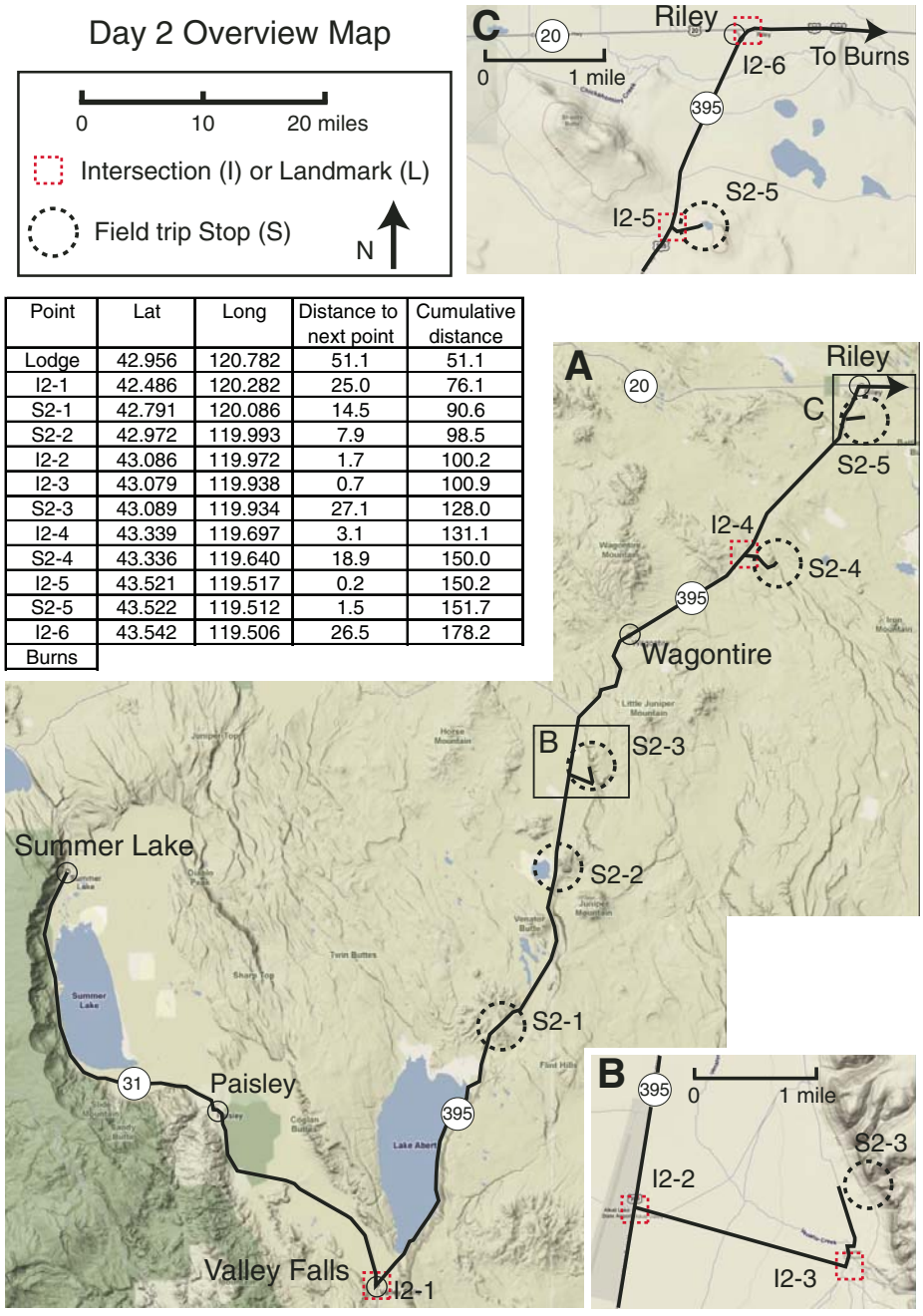

Point	Lat	Long	Distance to next point	Cumulative distance
Lodge	42.956	120.782	51.1	51.1
I2-1	42.486	120.282	25.0	76.1
S2-1	42.791	120.086	14.5	90.6
S2-2	42.972	119.993	7.9	98.5
I2-2	43.086	119.972	1.7	100.2
I2-3	43.079	119.938	0.7	100.9
S2-3	43.089	119.934	27.1	128.0
I2-4	43.339	119.697	3.1	131.1
S2-4	43.336	119.640	18.9	150.0
I2-5	43.521	119.517	0.2	150.2
S2-5	43.522	119.512	1.5	151.7
I2-6	43.542	119.506	26.5	178.2
Burns				

Figure 17. (A) Overview of Day 2 route with stop, intersection, and landmark coordinates. (B and C) Detailed stop locations. Stops are indicated with the letter S followed by the day and stop number. Key intersections (I) and prominent landmarks (L) are indicated. Distances are in miles.

The third and modern stage of High Lava Plains–northwest Basin and Range volcanism began ca. 10.5 Ma as the bimodal suite of widespread tholeiitic basalt and age-progressive rhyolites. At Abert Rim, basalt was erupted from Sawed Horn and Venator Butte; rhyolites include the Alkali Butte dome and the Rattlesnake Tuff.

Pre–Basin and Range Magmatism and Timing of Onset of Extension

The sweeping belts of intermediate composition magmatism that characterized the Basin and Range province prior to ca. 18 Ma are associated with extreme extension in many places (e.g., Armstrong and Ward, 1991; Seedorff et al., 1991; Stewart and Carlson, 1974). The wide distribution of middle Tertiary calc-alkaline magmatism of the Basin and Range has been attributed principally to (1) shallow subduction followed by delamination of the slab from the base of the lithosphere with attendant mantle upwelling (Best and Christiansen, 1991; Coney and Reynolds, 1977) and (2) extreme extension of thickened Laramide crust via low-angle detachment faulting (e.g., Armstrong and Ward, 1991; Wernicke, 1992). Modeled generation of these magmas involves mixing mantle-derived basalt with crustal rocks, in either a thickened, unextending crust (e.g., Best and Christiansen, 1991) or a ductile, rapidly extending lower crust (e.g., Gans et al., 1989).

The transition from middle Tertiary calc-alkaline magmatism to late Tertiary and Quaternary, bimodal basalt-rhyolite magmatism occurred between ca. 22 and 16 Ma in southeastern Oregon (Scarberry et al., 2007). In northern Nevada, peak Oligocene–Early Miocene (ca. 31–20 Ma) volcanism was bimodal and alkaline in composition (Colgan et al., 2006; Lerch et al., 2008), whereas time-equivalent, large-volume ignimbrite sheets that characterize the Basin and Range Province to the south and east are more intermediate and calc-alkaline in composition (Best and Christiansen, 1991). The ignimbrite sweep generally is ascribed to melting above a steepening or delaminating, subducting plate after a period of shallow-slab subduction. Yet the largely high-silica nature of the volcanism during this phase is unusual for typical convergent margin volcanism, and the east-trending alignment of the sweeping front is at odds to the more north-trending orientation of the convergent margin. Alternative models call on crustal thinning following Laramide shortening, and thickening, of the crust. In southeastern Oregon, middle to late Miocene magmatism is complex with respect to tectonic influences. On the one hand, part of the transition from intermediate calc-alkaline to basaltic volcanism is similar to what is observed during evolution of the margins of the Basin and Range Province in general (e.g., Christiansen and McKee, 1978). On the other hand, the region is potentially influenced by the Yellowstone hotspot (e.g., Camp et al., 2003; Jordan et al., 2004) or mantle flow related to northward migration of the Mendocino triple junction (e.g., Christiansen et al., 2002).

Driving Instructions

Leave the Summer Lake Lodge and proceed southeast 51.1 miles on Highway 31 to the intersection with U.S. Highway 395 (I2-1), just before the town of Valley Falls. Turn north and travel 25.0 miles to Coleman Hills roadcut (S2-1). Park on the left.

Stop 2-1. The Coleman Hills (42.791°N, 120.086°W)

Volcanic rocks of the Coleman Hills formed ca. 22 Ma (Scarberry et al., 2009). They crop out over an area of ~80 km^2 (Fig. 18). Topography represented by the Coleman Hills separates the Alkali Lake and Lake Abert basins (Fig. 19). The Coleman Hills are the eroded remnants of a composite volcano, consisting largely of intermediate composition lavas and intrusive rhyolite and dacite plugs, dikes and domes. Compositionally, the intermediate rocks are high-K, basaltic trachyandesite to trachyandesite (54.6–61.0 wt% SiO_2), trachyte (60.9–65.7 wt% SiO_2) and rhyolite (70.7–71.9 wt% SiO_2) (V.E. Camp, 2009, personal commun.; Scarberry et al., 2009). Field relations indicate that rhyolite and trachyte eruptions (stage 1) predate basaltic trachyandesite to trachyandesite volcanism (stage 2) throughout the volcanic complex. The volcano formed a paleotopographic high against which middle and upper Miocene volcanic units were disconformably deposited. This is consistent with the model of Mankinen et al. (1987), which suggests that as much as 1 km of relief existed locally prior to Middle Miocene Steens Basalt volcanism.

Our first stop is along U.S. Highway 395 where the road crests the rim north of the Lake Abert basin (Figs. 19 and 20). Here we will examine early Miocene dikes, sills, and volcaniclastic sediment that are exposed in a series of three roadcuts (Fig. 20). Many features in these outcrops point to locally explosive near-surface deposition in a wet environment. Some important observations include: (1) mafic dikes that are vesicular and exhibit quenched, glassy margins, (2) irregular contact boundaries between "sills" and tuff breccia and (3) dune forms in the lithic tuff, which consists of small ash- to lapilli-size lithic fragments and larger pumiceous lapilli that are rounded and reworked. Collectively, these relations suggest that stage 1 pyroclastic deposits mixed with sediment and accumulated in a shallow basin filled with water-saturated sediment that was then injected by mafic dikes during stage 2. Locally there is evidence to suggest that rhyolitic volcanism predated trachytic volcanism during stage 1 and that trachytic volcanism overlapped in time with stage 2 events.

Driving Instructions

Continue north on Highway 395 14.5 miles to Grays Butte access (S2-2).

Stop 2-2. Grays Butte (Stop at 42.972°N, 119.993°W)

Our second stop is at an alluvial fan on the southwest flank of Grays Butte, located ~15 miles to the north along U.S. Highway

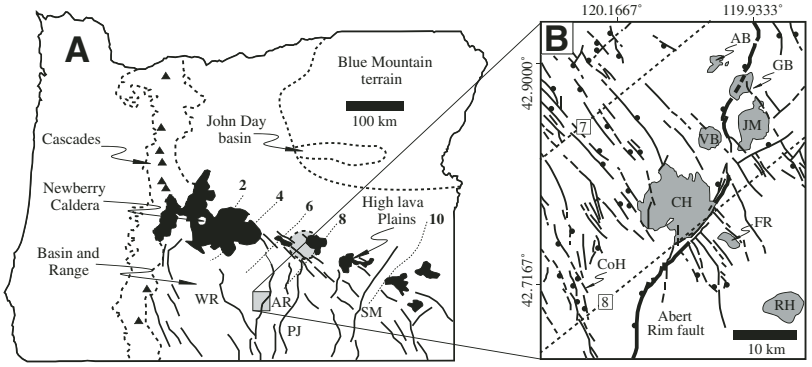

Figure 18 (Stop 2-1). Structural setting of Coleman Hills. (A) Regional structural grain of northwest Basin and Range showing location of field area to the south of the High Lava Plains, which coincides with black volcanic units and the silicic volcanic age progression (showing age in Ma). WR—Winter Ridge; AR—Abert Rim; PJ—Poker Jim Ridge; SM—Steens Mountain. (B) Local detail of the widely spaced, NNE-striking major Basin and Range faults and intersecting, abundant small NW-striking faults characteristic of the Brothers fault zone. AB—Alkali Butte; GB—Grays Butte; JM—Juniper Mountain; VB—Venator Butte; CH—Coleman Hills, FR—Flint Ridge; RH—Rabbit Hills. Box shows area of Figure 17.

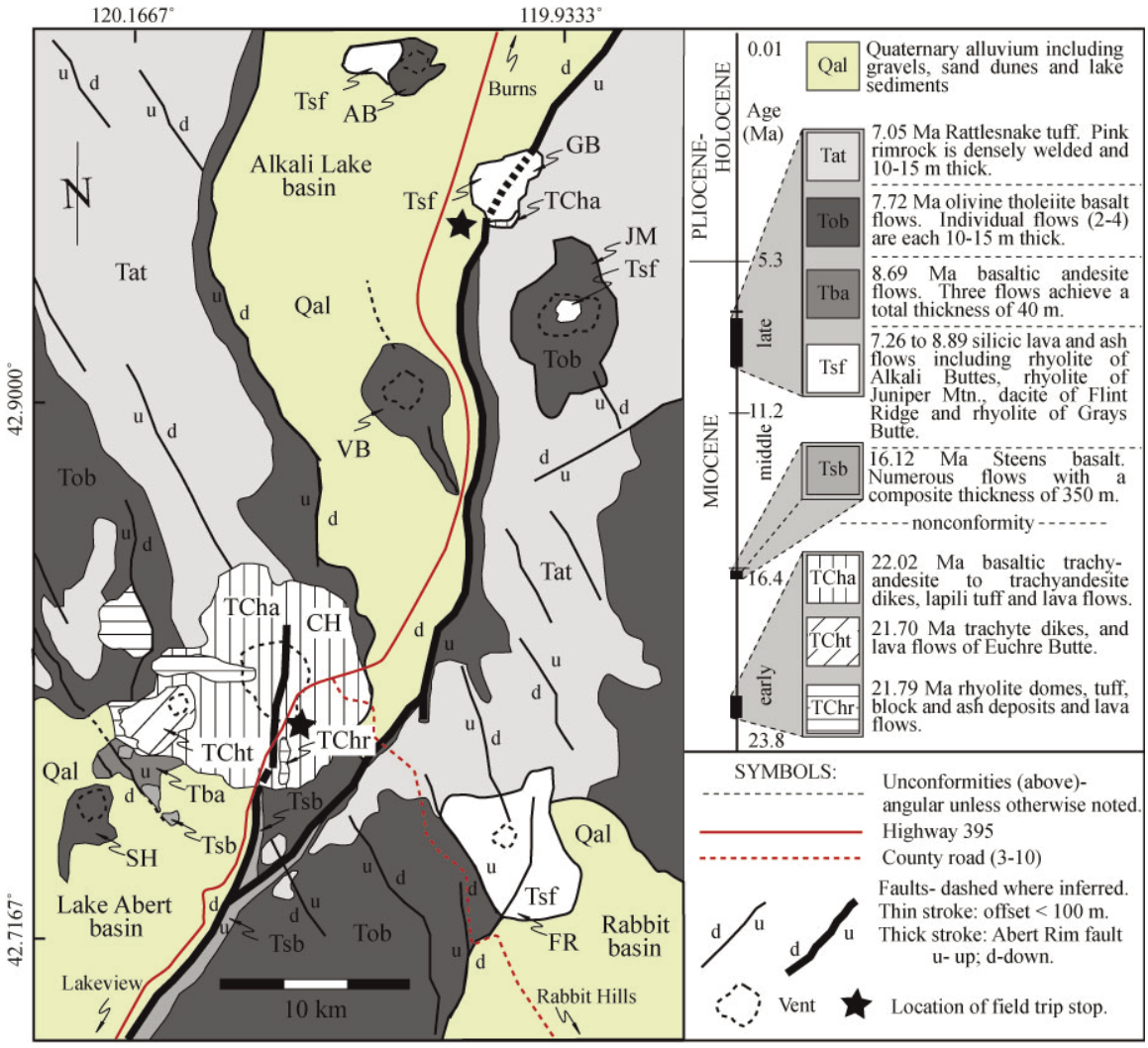

AB- Alkali Butte, **FR**-Flint Ridge, GB- Grays Butte, **JM**- Juniper Mountain, **SH**-Sawed Horn, **VB**-Venator Butte,

Figure 19 (Stop 2-1). Simplified geology of the Coleman Hills. From Scarberry et al. (2009).

395 heading toward Burns (Figs. 17 and 19). Stop on the east side of the road 0.4 mi north of the Alkali Lake Station. From the road we can see a complicated contact relation between Grays Butte and the layers exposed in the footwall of Abert Rim just south of the butte (Fig. 22A). If time permits, we will hike up the fan to look at these rocks more closely (Fig. 22B).

New $^{40}Ar/^{39}Ar$ ages from this area indicate that the Grays Butte (8.9 Ma, unpublished) intrusion occurred during the earliest stage of Late Miocene silicic volcanism in this region (ca. 7.5–9 Ma), which coincided with formation of the southern segment of the Abert Rim fault (Figs. 21 and 22A). A mafic lava located at the top of the tilted section along the side of Grays Butte (unit 3;

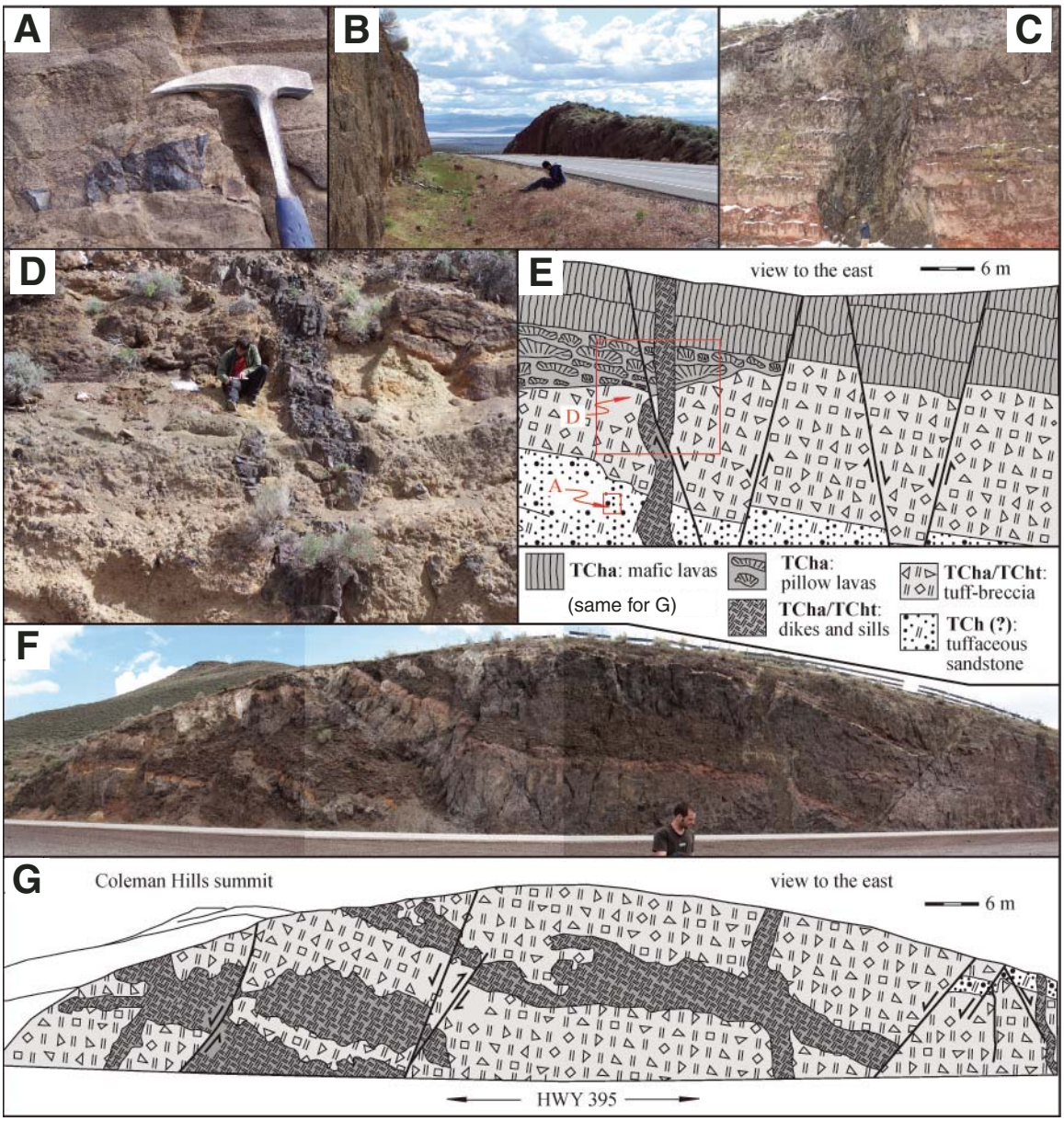

Figure 20 (Stop 2-1). Faults and dikes in the Coleman Hills volcano. (A) Detail of tuffaceous sandstone (TCh). Location of photo shown on panel E. (B) View looking south to Lake Abert from the roadcut in 395 of the stop. Lake Abert in the distance is also in the hanging wall of the Abert Rim fault and sits topographically lower than the Coleman Hills. (C) Cross-cutting relationship between older dikes and sills and younger tuff and breccia within the Coleman Hills volcano. (D) Offset Coleman Hills–aged dike, which is shown in the interpretive line drawing of roadcut on east side of highway at Stop 2-3. (F and G) Photograph and interpretive line drawing of roadcut on east side of Highway 395 at Stop 2-3 showing the intrusive relationship between dikes and sills into tuff and breccia of the Coleman Hills, all of which are cut by a younger generation of normal faults.

Fig. 22B) yielded an Early Miocene age (21.9 Ma, unpublished), contemporaneous with stage 2 trachyandesite volcanism at the Coleman Hills. This age information is significant for two reasons: (1) The sedimentary units (units 1 and 2; Fig. 22B) in the tilted section, which exhibit sorting and rounding consistent with deposition in a fluvial channel migrating across a fan, are representative of the landscape prior to Early Miocene volcanism in this region, and (2) The lavas that are unconformably deposited against the tilted section (Tob; Fig. 22A) must be between 7 and 9 Ma because they are overlain by the 7.05 Ma Rattlesnake Tuff and were not deformed by the intrusion. The significance of this is that Middle Miocene Steens Basalt is not exposed here, whereas the unit is >300 m thick ~30 km to the south.

DAY 2, AFTERNOON. MAGMATIC AND TECTONIC IMPLICATIONS OF THE RATTLESNAKE IGNIMBRITE EVENT

Summary of Harney Basin Ignimbrites

The Rattlesnake Tuff is one of three widely recognized ignimbrite units that have their sources in or near the Harney Basin. The lowermost is the 9.7 Ma Devine Canyon Ash-Flow Tuff, which is separated from the overlying 8.4 Ma Prater Creek Ash-Flow Tuff by poorly exposed tuff and tuffaceous sedimentary rocks. The Prater Creek is overlain by equally poorly exposed tuff and tuffaceous sedimentary rocks, which in turn are overlain by the 7.05 Ma Rattlesnake Tuff. These ignimbrites, each with an estimated volume of hundreds of cubic kilometers, represent the greatest outpouring of rhyolite in the High Lava Plains. In contrast, many ignimbrites of the Snake River–Yellowstone trend are larger by orders of magnitude, with volumes of thousands to hundreds of thousands of cubic kilometers (Pierce and Morgan, 1992).

The focus of the westward-migrating silicic volcanic trend between ca. 8 and 7 Ma was the western Harney Basin. Erupted products include not only the Prater Creek, Rattlesnake Tuff, and smaller Buckaroo Lake Tuff but also numerous dome complexes such as Horse Mountain, Alkali Butte, Burns Butte, and eastern Juniper Ridge. This episode also corresponds to a time of widespread basalt volcanism. The coincidence of the basalt pulse with the locus of westward-migrating silicic volcanism likely accounts for the exceptionally productive volcanic activity.

Devine Canyon Tuff

The Devine Canyon Tuff is crystal rich and originally covered more than 18,600 km^2 of southeastern Oregon, with a total volume of ~195 km^3 (Greene, 1973). It is characterized by 10%–30% phenocrysts of alkali feldspar and quartz, with sparse

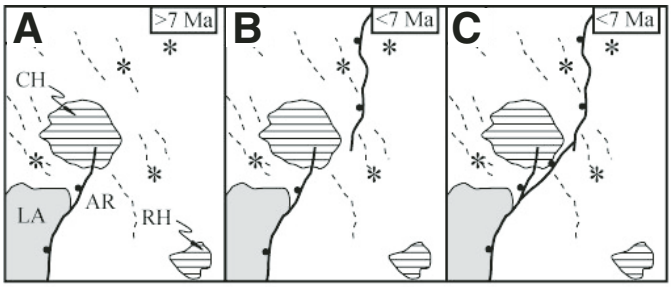

Figure 21 (Stop 2-2). Cartoon depicting the sequential development of faults along Abert Rim near the Coleman Hills volcano. A tilting event of rocks by northwest-trending faults in the hanging wall of the Abert Rim fault prior to 7 Ma, faults that are cut by the Abert Rim fault, suggests that the Abert Rim fault had formed to the south of the Coleman Hills before 7 Ma (Scarberry et al., 2009). A prominent topographic low marks along the Abert Rim fault to the east of the Coleman Hills implies the fault grew the fault grew by linking fault segments to the north and south of the Coleman Hills (B and C).

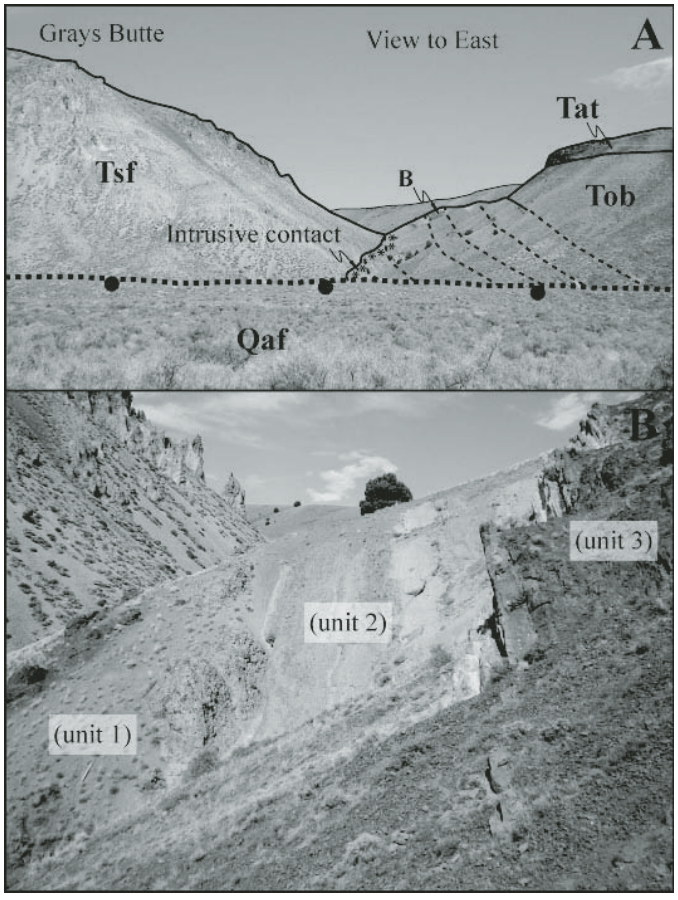

Figure 22 (Stop 2-2). Geological field relations at Grays Butte. (A) View east 1 km to contact of Grays Butte (left) and older strata in Abert Rim escarpment. Qaf—alluvial fan deposits; Tsf—silicic flows; Tat—ash-flow tuff; Tob—olivine basalt. (B) Photo of upper Oligocene volcaniclastic strata deformed by Grays Butte dome. Units 1 and 2 are fluvial deposits overlain by a mafic lava (unit 3).

clinopyroxene. It varies from nonwelded to densely welded; most outcrops are of greenish-gray stony devitrified tuff. Thickness is ~30 m near the type section ~0.5 km northeast of the confluence with Poison Creek and corresponds to observed maximal thicknesses (Greene, 1973). A $^{40}Ar/^{39}Ar$ age of 9.74 ± 0.02 Ma was obtained from sanidine separates (Jordan et al., 2004).

Prater Creek Tuff

The Prater Creek Ash-Flow Tuff is mainly a devitrified, crystal-poor ash flow tuff. Exposures of the type section on the walls of Poison Creek (Designated by Walker, 1979) can be seen from U.S. Highway 395. There the maximum thickness is 12 m; lithologic variations can be seen in reference sections in Prater Creek, ~5 km east of Poison Creek. The type section consists chiefly of pale-grayish-red, devitrified tuff with grayish-pink gas cavities to ~2 cm in diameter. Flattened, devitrified pumice fragments are present throughout but are not abundant. Alkali feldspar and quartz are sparse, and the tuff contains rare lithic fragments (Walker, 1979). Devitrified whole-rock tuff gave an age of 8.41 ± 0.16 Ma (Jordan et al., 2004).

Rattlesnake Tuff

The Rattlesnake Tuff is nonwelded to densely welded pumice-to-ash-rich tuff with spherulitic, lithophysal, devitrified and vapor-phase crystallization zones. Phenocryst content is ≤1% throughout the bulk of the tuff; phenocrysts are mainly alkali-feldspar, Fe-rich clinopyroxene, quartz, magnetite, and fayalite. Where pumiceous, the tuff commonly has distinctive white, gray, black, and banded pumice lapilli and bombs set in a salt-and-pepper matrix of white and gray glass shards. Typically the tuff occurs as 10–20-m-thick cliff-forming rimrock; maximum thickness is ~70 m. The tuff likely originally covered 35,000 km^2. Weighted mean age of 15 single-crystal $^{40}Ar/^{39}Ar$ analyses of alkali feldspar yielded an age of 7.05 ± 0.01 Ma (Streck and Grunder, 1995). Maximal run-out distance, as based on today's outcrop remnants, is ~150 km to the north and south from its likely source area in the western Harney Basin (Streck and Grunder, 1995). For its size, the Rattlesnake Tuff is among the most far-traveled ignimbrite known.

The Rattlesnake Tuff is an important case study for addressing the effect of magmatism on the crust. The stages in its petrogenesis require either thermal or material inputs from basalt and so are evidence for "basaltification" of the crust beneath the High Lava Plains.

Basalt is required for Rattlesnake rhyolite genesis in two main ways:

1. Energy, likely in the form of basalt intraplating of the crust, is required to melt the mafic wacke protolith shown by (Streck, 2002) to be plausible protolith for least-evolved "rhyolite E" of the Rattlesnake Tuff.

2. Heat is required to thermally sustain the crystal-poor rhyolite and the fractionation, by 50%, of rhyolite E to produce rhyolites D, C, B, and finally A (Streck and Grunder, 1995).

In turn, the Rattlesnake Tuff provides a density filter that traps mafic magma, causing extensive fractionation and recharge beneath the chamber, as represented by trace-element-enriched basaltic andesite inclusions in the tuff. This basaltic andesite composition contributes to basaltification and also serves as a mixing end member for scarce dacite pumice in the tuff (Streck and Grunder, 1999).

Evidence for crustal basaltification in the Harney Basin area is supported by increasing basalt-like isotopic characteristics among successively younger rhyolites in western Harney Basin (Streck and Grunder, 2008). Finally, the decreasing basinward dip of volcanic units from Devine Canyon time to ca. 2 Ma, when flat-lying basalt ponded in the basin (such as Wright's Point lava flow (Jordan et al., 2004), is consistent with increasing of crustal density by basalt intraplating in time. Emplacement of a gabbro layer into the crust has been modeled to explain the depressed topography in the Snake River Plain. The intrusion of magma may also have accommodated some extension in lieu of faulting.

Driving Instructions

Return to Highway 395 and continue north. Drive 7.9 miles north to intersection I2-2 and turn right (east). Follow the road 1.7 miles to I2-3 and turn left (north). Go 0.7 miles and park (S2-3).

Stop 2-3: Rattlesnake Tuff and basalt at Abert Rim (43.11°N, 119.95°W)

In the escarpment near the cow camp we will look at the Rattlesnake Tuff and the basalts that underlie and intrude it.

The Abert Rim escarpment diminishes in relief to the north and curves northwest, becoming "Alkali Rim" (informal geographic name denoting the topographic rim that bounds the east side of Alkali Valley). Exposed in the escarpment is a thick section of Rattlesnake Tuff underlain, overlain, and invaded by high-alumina olivine tholeiite. The base of the tuff is a distinct thin white, near-horizontal band. The tuff overlies inflated pahoehoe basalt that overlies another ignimbrite, likely the Prater Creek Ash-Flow Tuff, based on its stratigraphic position and lack of crystals. The Rattlesnake Tuff grades abruptly upsection from vitric nonwelded, incipiently welded, partially welded, and densely welded facies to a devitrified, lithophysal, and vapor-phase altered facies that makes up most of the section. Three basalt sills intrude the tuff. Near the northern termination of the ~1-m-thick upper sill, pipe vesicles are developed at the lower and upper contact. Intruding features include ripped-up pieces of Rattlesnake Tuff and well-developed vesicle sheets near the upper contacts of both the thick middle sill and the upper sill.

Driving Instructions

Return to Highway 395 and continue north. The highway crosses numerous northwest-striking faults that increase in abundance as Abert Rim loses topographic expression and dies

out in the plain. Drive 24.7 miles to intersection of "Alec Butte Road" (I2-3), gravel, and turn right (east). This turn is 11.0 miles north of the town of Wagontire. Follow the road to edge of the northwest-trending rimrock, ~3.1 miles and park (S2-4).

Stop 2-4. Alec Butte and the Brothers Fault Zone (43.336°N, 119.640°W)

This stop is to consider the structure and timing of the Brothers fault zone. U.S. Highway 395 crossed into the Brothers fault zone at 43.3°N, 119.8°W, roughly 8 km southwest of the turnoff to this stop. The Brothers fault zone is a regionally extensive fault system that separates the principal north-northeast–striking Basin and Range extensional faults in south-central Oregon from less extended terrain to the north. At its eastern edge, the Brothers fault zone marks the southern edge of the modern Harney Basin. There is 150–180 m of topographic relief between the Brothers fault zone and the Harney Basin on the north. Faults of the Brothers fault zone strike mainly northwest. Vertical offset is typically down to the northeast (Fig. 6) (Lawrence, 1976; Trench, 2008).

At this stop, the Alec Butte cinder cone (Qtp) (Fig. 23) conformably overlies an olivine basalt that forms the rim rock of fault escarpments to the north of the stop, which we correlate with a 5.68 Ma olivine basalt dated to the northwest of Alec Butte (Tob, Jordan et al., 2004; Trench, 2008). The stop is in

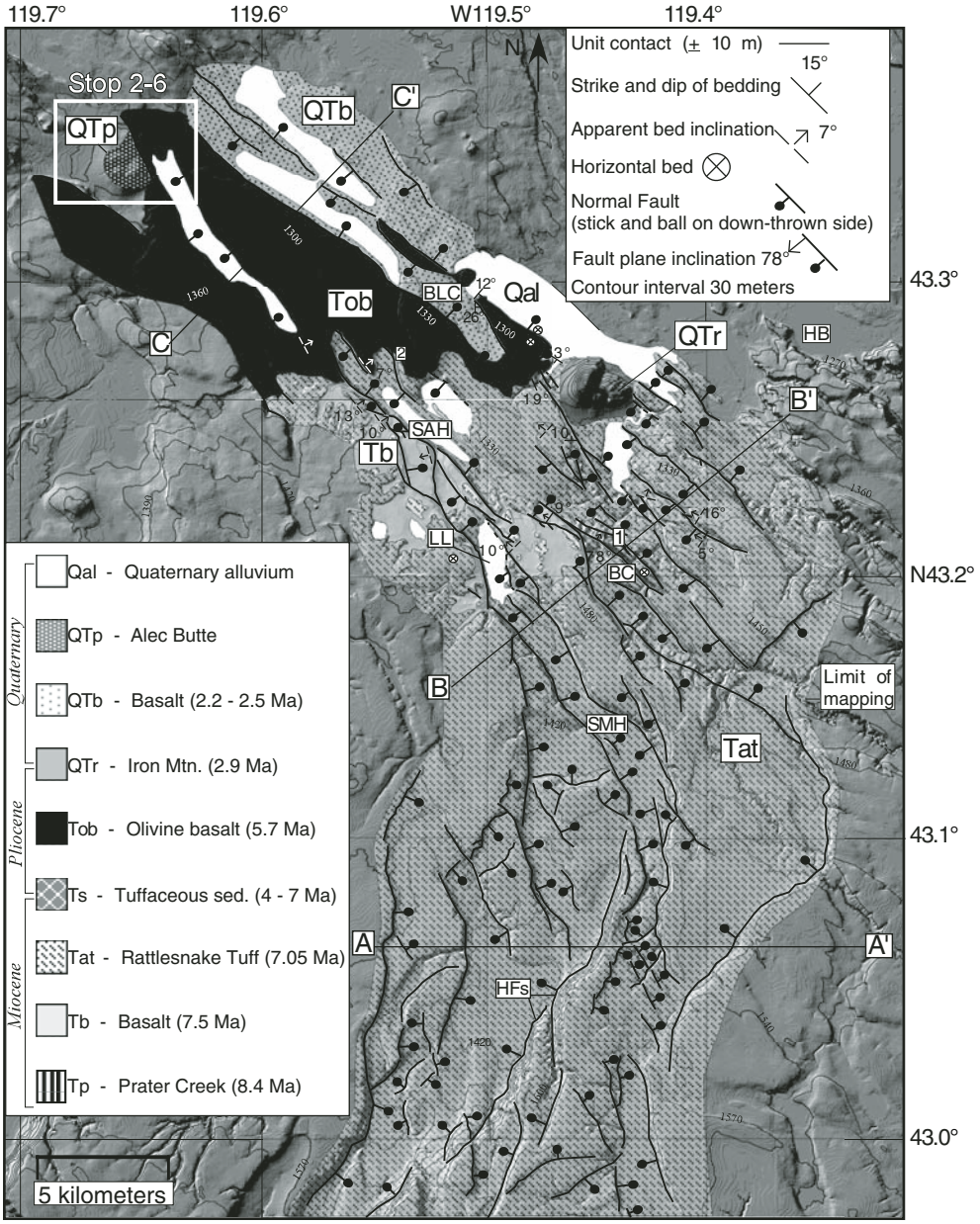

Figure 23 (Stop 2-4). Geologic map of the Brothers fault zone near Alec Butte. BC—Buzzard Canyon; BLC—Black Canyon; SMH—Smokey Hollow; LL—Lunch Lake; HFs, Hart Mountain fault system; HB—Harney basin; SAH—Sand Hollow. Cross sections A–A′, B–B′, and C–C′ are shown on Figure 22. From Trench (2008). Unit ages are from Jordan et al. (2004) and Streck and Grunder (1995).

the footwall block of a fault that defines the southwest margin of the Alec Butte graben, a topographic low within the Brothers fault zone. Topographic relief is ~60 m, which is a proxy for the minimum and normal separation across the fault (Fig. 24). Faulting in the Brothers fault zone postdates the Tob and Qtp units because they are cut by the fault. To the southeast, the 2.89 Ma rhyodacite of Iron Mountain (Jordan et al., 2004) is mostly unbroken by northwest striking faults (Trench, 2008). Iron Mountain is the only silicic dome known to be younger than the age-progressive silicic volcanism of the High Lava Plains. Dating of Alec Butte is planned. If Alec Butte is younger than Iron Mountain, then deformation in the Brothers fault zone occurred on some faults after 2.89 Ma. The total amount of extension across the Brothers fault zone is no more than 63 ± 10 m, assuming a fault dip of 70°. Forty four meters of that extension occurs across the Alec Butte graben. Sequential restoration of cross sections indicate that down-to-the-northeast faulting extensional faulting in the Brother fault zone predates northward propagation of Basin and Range faults (Scarberry et al., 2009; Trench, 2008).

Regional Tectonic Models

The long-standing model for termination of extensional faulting in the northwestern Basin and Range is the right-lateral transform model proposed by Lawrence (1976). At odds with the model is the prominent apparently normal throw on Brothers fault zone faults. More recent work indicates a dextral oblique-normal sense of slip, in which the ratio of strike-slip to dip-slip separation is ~1:1, characterizes faulting in the Brothers fault zone (Trench, 2008). A piercing point measured across one fault in the fault zone demonstrates that the strike-slip component in small and roughly the same as the dip-slip separation (Trench, 2008). Field relations demonstrate that north-northeast striking faults of the Basin and Range do not end simply at northwest-striking Brothers fault zone faults. Rather, the two fault sets mutually crosscut each other, and the north-northeast-striking faults die out to the north into the Brothers fault zone (Fig. 6). For range-front faults west of Steens Mountain, relations are consistent with a model where northwest-trending horsetail splays at the tips of Basin and Range faults intersect preexisting northwest-striking faults of the Brothers fault zone as the Basin and Range propagates northward through time (Scarberry et al., 2009; Trench, 2008).

A model of northward-propagating extensional fabric, with the Brothers fault zone representing horsetail fractures, provides a reasonable explanation of regional fault patterns, crosscutting relations, topographic gradients, and the distribution of extension in the northwest Basin and Range and Brothers fault zone (Fig. 25). However, the model does not adequately explain the independent

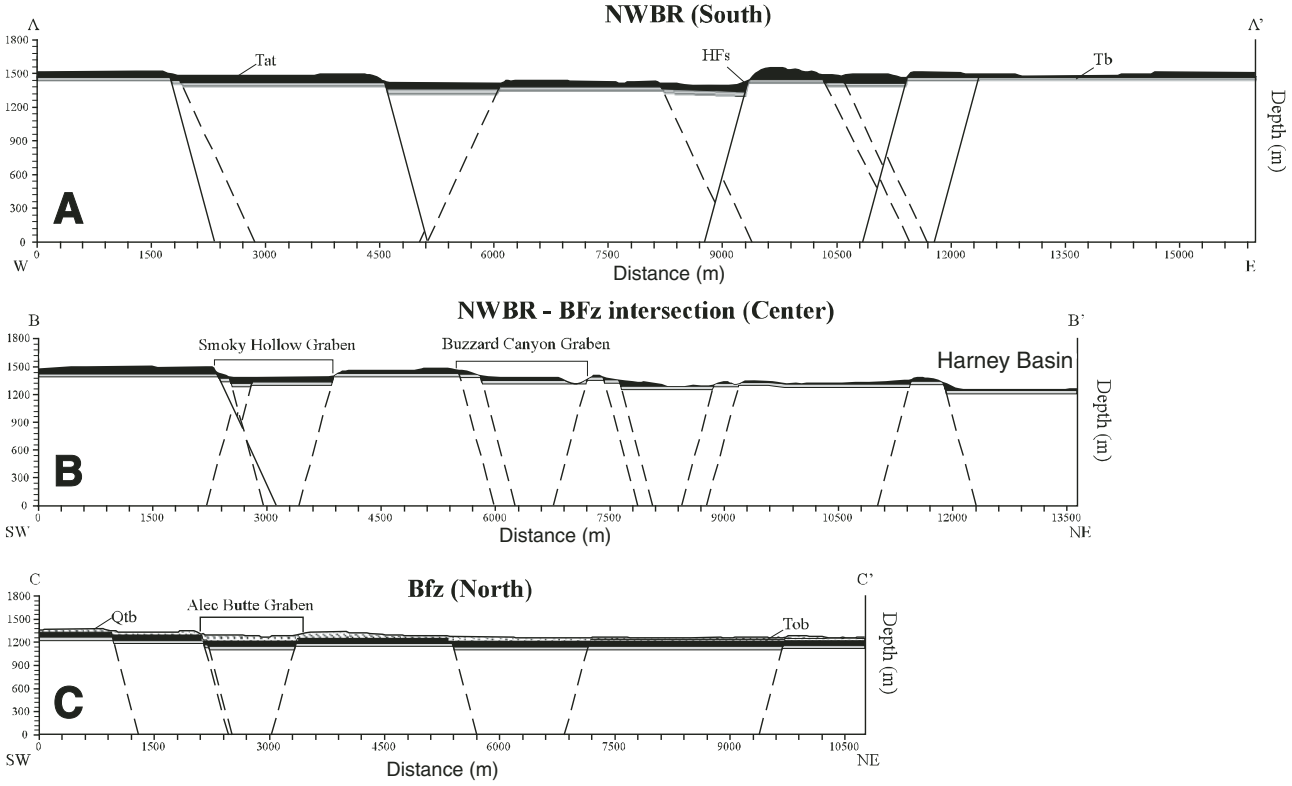

Figure 24 (Stop 2-4). Cross sections for part of Brothers fault zone shown on Figure 23. Dashed lines are northwest-striking faults and solid lines are north northeast-striking faults. Unit patterns as in Figure 23.

slip history implied from the cross-section reconstructions. Regional structural relations fit well in a model for regional active deformation that combines fault lengthening to the north-northeast with fault-tip deformation consumed on northwest-trending faults and pole-of-rotation-driven plate-scale deformation.

Driving Instructions

Return to Highway 395 and continue north 15.8 miles to the road that leads to a cinder quarry (I2-4) and turn right (east). Travel 0.2 miles to the quarry (S2-5).

Stop 2-5 (optional). Overview of mafic volcanism from near Shields Butte (43.522°N, 119.512°W)

This stop is near the western margin of the Harney Basin and, from here, several mafic vents and lava sequences can be viewed that span a wide range of compositions over a small area. Late Miocene to Quaternary mafic volcanism of the western Harney Basin is of three types defining two trends. The regional HAOT is dominant and evolves to enriched basaltic trachyandesite through recharge and fractionation, as represented by the mafic inclusion of the Rattlesnake Tuff and the basaltic trachyandesite of Paiute Butte. Another trend is toward calc-alkaline basaltic andesite through crustal contamination, as well as potential recharge and crystal fractionation.

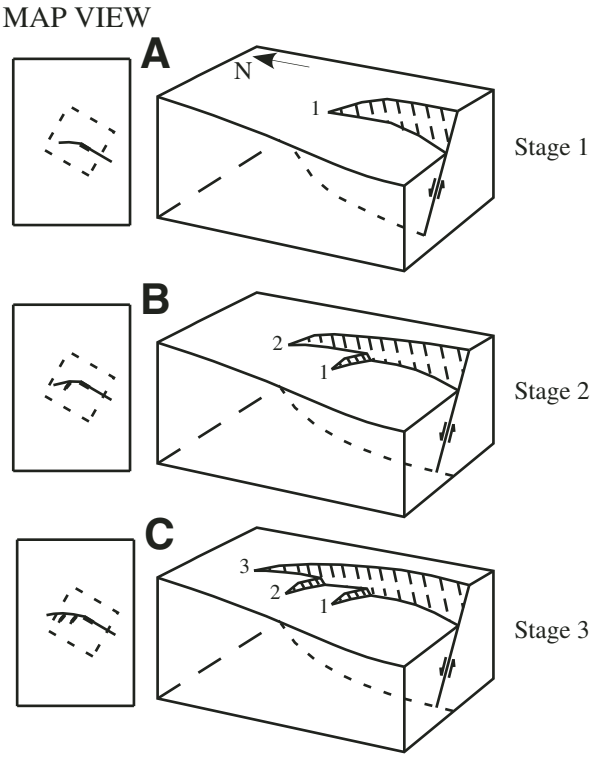

Figure 25 (Stop 2-4). Block diagrams showing schematic sequence of fault propagation. (A) Normal fault propagates along strike, with incipient horsetail splay (labeled "1") at termination. (B) Continued propagation truncates the initial horsetail as termination becomes new incipient splay ("2"). (C) Continued fault propagation truncates earlier horsetail fractures (from Trench, 2008, modified from Crider, 2001).

Shields Butte, 2.4 km south-southwest of Riley, is a pile of lavas—many agglutinated—and is part of the scoria cone exposed here. Shields Butte is disrupted by Brothers fault zone structures. Shield Butte basaltic andesite contains 52.8% SiO_2 and shows calc-alkaline affinity.

The view from the hill that makes the east side of the quarry includes (Fig. 26) (1) Palomino Butte (azimuth 104°, age 6.35 ± 0.03 Ma); (2) Blacktie Butte (subdued hill at azimuth 96°), a mafic vent of very incompatible trace-element–enriched trachyandesite; (3) Oakerman Butte (azimuth 58°, age 5.25 ± 0.09 Ma), a mafic vent of basaltic trachyandesite that is transitional between calc-alkaline and the most enriched basaltic trachyandesite; (4) fault scarps (azimuth 40°, age 7.60 ± 0.11 Ma at base) in which are exposed a sequence of calc-alkaline basaltic andesite flows that grade into basalt near the base of the section, (5) Dry Mountain (338°), a mid-Miocene andesitic center (Fig. 4), Shields Butte (304°), and Juniper Ridge (245°–270°, where a sample from sample from the eastern edge is 6.90 ± 0.02 Ma, and a sample on the west margin is 5.78 ± 0.02 Ma). Paiute Butte (254°, age 2.37 ± 0.04 Ma) is the sharp butte that peaks up behind Juniper Ridge; it erupted lavas of very enriched basaltic trachyandesite.

Driving Instructions

Return to Highway 395 and continue north 1.5 miles to the junction with U.S. Highway 20 at Riley (I2-5). The likely buried source region of the Rattlesnake Tuff lies to the south of this junction (Fig. 4). Drive east ~26.5 miles to motels in Burns. Check in and meet for dinner and a geophysical overview.

Overview of High Lava Plains Project Geophysical Results

The goal of the High Lava Plains seismic experiment is to understand the dynamics of the Juan de Fuca subduction system as it relates to the evolution of tectonomagmatism across the backarc, including flood basalt of the Columbia River Basalt Group, volcanism across the High Lava Plains, and the time-progressive Newberry and Yellowstone hotspot tracks. To provide images of the regional crust and mantle, the High Lava Plains seismic team has utilized broadband seismic data from several arrays, including the USArray Transportable Array and the 118 stations of the High Lava Plains seismic array. The High Lava Plains seismic array's first stations were deployed in January 2006, and the network is slated for demobilization in September 2009.

Images from body wave tomography (Roth et al., 2008) and upper mantle discontinuity receiver function results (K.C. Eagar, 2009, personal commun.) are broadly consistent with each other and demonstrate that the Juan de Fuca slab is well

imaged and extends to depths of ~500 km, perhaps deeper. Zones of focused reduced seismic velocities are evident beneath both Newberry Volcano and the surface expression of the Columbia River Basalt Group. At lower-mantle depths (700 km and deeper), we image planar deep structures that may correspond to a slab break that occurred ca. 15 Ma. We find no evidence for mantle plume-type structures across the High Lava Plains–Newberry–Columbia River Basalt Group region. Similarly, we find no evidence for a zone of low velocities beneath the Juan de Fuca slab. Further, we demonstrate, by a thorough series of resolution tests, that the absence of a slab signature in central Oregon, interpreted by some groups as a "hole" in the slab, is instead an inversion artifact due to imperfect ray coverage and the presence of the reduced velocity zone coincident with Newberry Volcano.

DAY 3, MORNING. MODERN AND PROTO-HARNEY BASIN AND THE HIGH LAVA PLAINS PROVINCE (FIGURE 27)

Deposits and structures preserved in a set of north-striking tilt blocks in the Crowcamp Hills along the eastern margin of the Harney basin east of Burns, Oregon (Figs. 6 and 28), herein referred to as the Crane basin, reveal some of the earliest evidence of extensional deformation in the northwestern Basin and Range. Stratigraphic relationships of sediments accumulated in the Crane basin, a regionally extensive depocenter, records initial fault development after eruption of the 16 Ma Steens Basalt, but prior to High Lava Plains volcanism. The basal contact of these fluvial and lacustrine deposits unconformably overlies the ca. 16.6 Ma Steens Basalt and a suite of ca. 12 Ma rhyodacite intrusions. Fluvial and lacustrine deposits thicken toward normal faults bounding individual half graben, which demonstrates that extension-related basins formed prior to eruption of the 9.7 Ma Devine Canyon Tuff (Stop 3-1). Extension-related subsidence in the Crane basin continued after Devine Canyon time and through eruption of the ca. 7.1–7.2 Ma Drinkwater Basalt (Fig. 28) (Greene et al., 1972). A suite of east-trending faults discontinuously exposed along the valleys of Crane Creek and the south fork of the Malheur River separate relatively little extended domains from more extended domains. Because these faults are orthogonal to the principal normal faults and presumably parallel to the regional extension direction, we refer to the suite of faults as the Crane shear zone and interpret

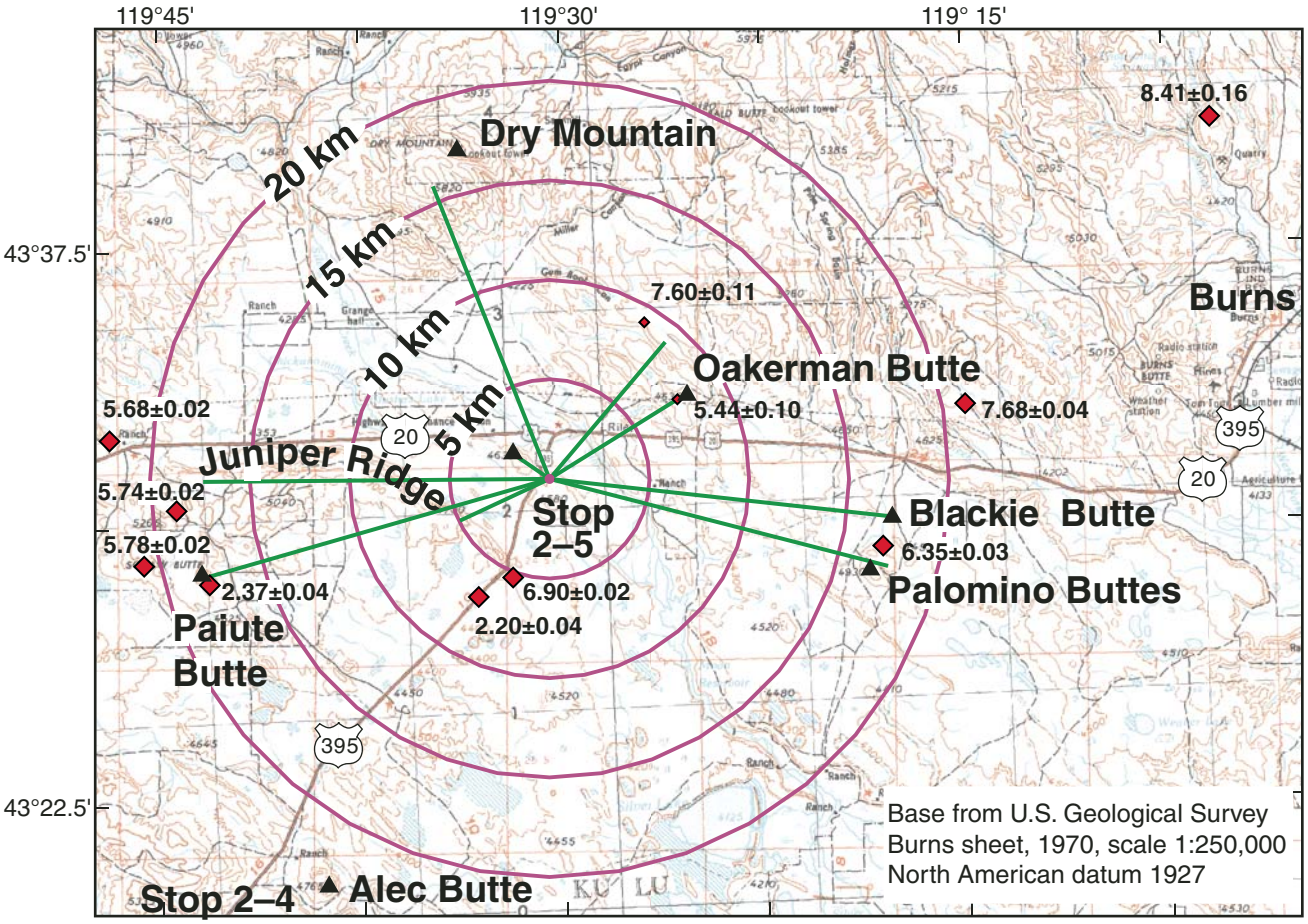

Figure 26 (Stop 2-5). Wheel diagram for view from Shields Butte. Inspired and constructed by D. Sherrod.

it as a transfer fault zone (Stop 3-2) (Faulds and Varga, 1998). After ca. 7 Ma, deformation shifted to the west, which resulted in formation of the Harney Basin. Deformation in the Crane basin largely ceased after ca. 7 Ma (Stop 3-3).

Driving Instructions

To reach the Day 3 morning stops, drive east from Burns ~28 miles on Oregon Highway 78 toward Crane. In Crane, go east at the intersection (I3-1) on the Crane-Venator Road.

About four miles east of Crane, you leave Harney basin, an internally-drained basin. Low topographic divides on the east side of the basin isolate the Harney basin from the Malheur River system. In Pleistocene time, however, pluvial Malheur Lake overtopped the divides several times (Dugas, 1998). The road passes through Crane Creek Gap, one of the divides, and continues east along Crane Creek, a tributary of the South Fork of Malheur River. Venator lies at the tributary junction of Crane Creek and the south fork of the Malheur River, the other major outlet of Pluvial Malheur Lake (L3-1), 17.5 miles beyond Crane. Continue 1.9 miles beyond Venator to the Crane basin overview (S3-1).

Stop 3-1. Stratigraphic Relationships within a Crane Basin Half Graben (43.372°N, 118.291°W)

Growth strata that both predate and postdate the deposition of the Devine Canyon ignimbrite illustrate the timing of faulting and deposition in the Crane basin (Fig. 29). From this vantage point the prominent marker beds are the Devine Canyon Tuff in the mid-slope and the Drinkwater Basalt forming the rim rock. Fluvial and lacustrine deposits underlie the recessive slopes below the two marker beds. Hanging wall strata thickening westward toward an east-dipping normal fault, which is particularly clear in the change in thickness of the sediments between the two marker beds. A 4° angular discordance between the Devine Canyon Tuff (Tdv) and the Drinkwater Basalt (Tdw) (Fig. 29) indicates progressive tilting of the half-graben strata during deposition. To the east, out of frame of Figure 29, units pinch out due to onlap onto the Steens Basalt (Tba) and a younger rhyodacite intrusion (Trd). A period of subsidence beginning after Steens Basalt eruption at 16.5 Ma and continuing through eruption of the capping Drinkwater Basalt (Tdw) is revealed by these relations. We obtained a $^{40}Ar/^{39}Ar$ plateau age of 7.25 ± 0.09 Ma (Fig. 30) from an out-

Point	Lat	Long	Distance to next point	Cumulative distance
Burns			28.0	28.0
I3-1	43.420	118.589	17.5	45.5
L3-1	43.348	118.304	1.9	47.4
S3-1	43.372	118.291	6.4	53.8
S3-2	43.436	118.238	20.2	74.0
S3-3	43.390	118.491	102.0	176.0
L3-2	43.674	120.237	4.9	180.9
I3-2	43.712	120.318	7.3	188.2
S3-4	43.774	120.281	End	

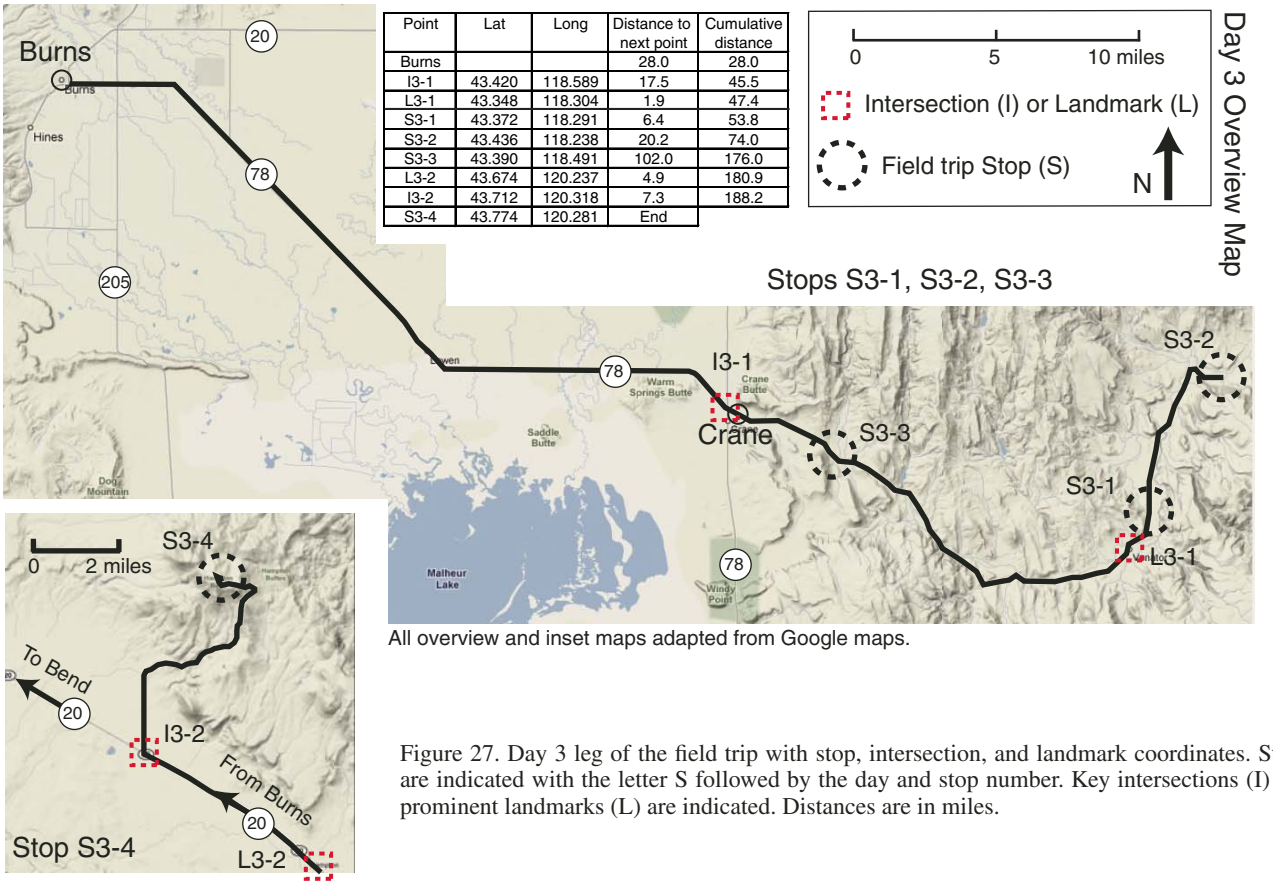

All overview and inset maps adapted from Google maps.

Figure 27. Day 3 leg of the field trip with stop, intersection, and landmark coordinates. Stops are indicated with the letter S followed by the day and stop number. Key intersections (I) and prominent landmarks (L) are indicated. Distances are in miles.

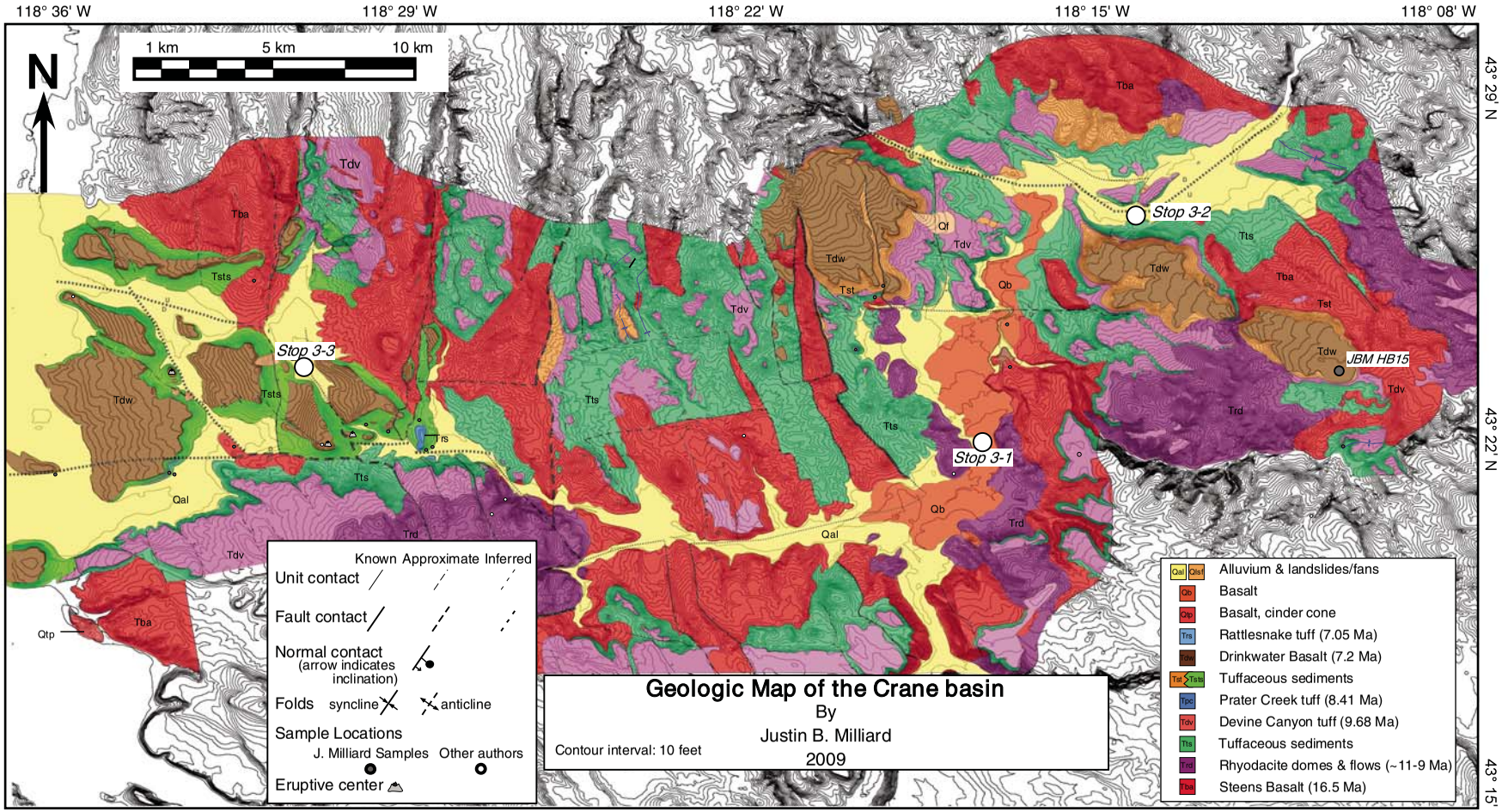

Figure 28. Draft of a new geologic map of the Crane basin (Stops 3-1, 3-2, and 3-3; Fig. 27). This is a preliminary version that will form the basis of J. Milliard's M.S. thesis. Sample JBM HB15 is plotted (Fig. 30).

crop near this stop, which agrees well with a published 7.10 ± 1.12 K-Ar age (Greene et al., 1972).

Driving Instructions

Continue driving north and east 6.4 miles to Crane Creek Shear Zone (S3-2).

Stop 3-2. Evidence for Differential Extension and the Presence of the Crane Shear Zone (43.436°N, 118.2378°W)

Structural relationships to the north and south of the road at this stop provide evidence for the presence of an east-trending transfer fault, one of the faults of the Crane shear zone. The road runs parallel and on the south side of the south fork of the Malheur River. Facing to the north one sees two tilted panels capped by the Devine Canyon Ash-Flow Tuff, which define the dip slopes of the low hills on the north side of the river (Fig. 31). A north-striking east-dipping normal fault dropped the eastern tilt block relative to the western block (Figs. 31 and 32). In detail, an east-striking fault with a small vertical separation (10s of meters) offsets the Devine Canyon Tuff in the tilt blocks. Facing to the south, a continuous stratigraphic sequence from the Steens Basalt (the outcrop in the foreground of the photo; Fig. 32) up-section to the Drinkwater Basalt is exposed. Discontinuous outcrops of the Devine Canyon Tuff in the midslope and the continuous rimrock of the Drinkwater Basalt indicate that the north-striking faults do not continue to the south of the river (Fig. 28). The observation that north-striking faults do not continue across the south fork of the Malheur River, that units on the south side are neither tilted nor faulted, that tilted Devine Canyon and older sediments are juxtaposed against the Steens basalt across the river, and that there is a small fault with an east strike form the basis of the interpretation that the valley bottom is occupied by an east-striking transfer fault zone, the Crane shear zone.

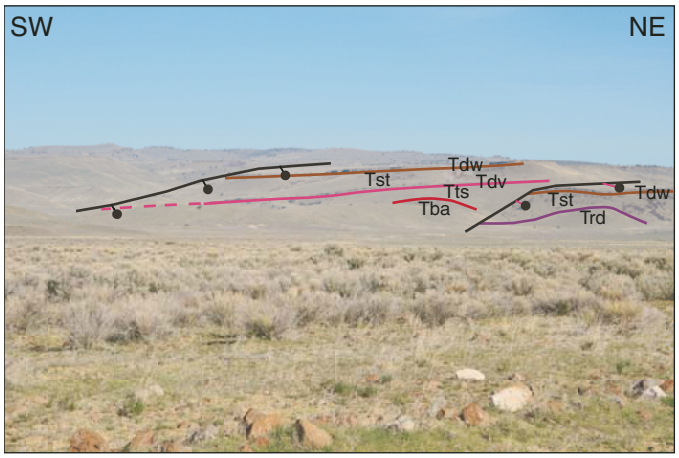

Figure 29 (Stop 3-1). Oblique cross-sectional view to the northwest of the stratigraphic relationships that typify half grabens within the Crane basin. Note that units thicken toward the western, basin-bounding fault side of the basin. This thickening is interpreted to reflect fault growth during deposition. Units include Tba (red line)—Steens Basalt; Trd (purple line)—rhyodacite intrusion; Tts—tuffaceous sedimentary rocks; Tdv (pink line)—Devine Canyon Ash-Flow Tuff; Tst—sedimentary and tuffaceous rocks, and Tdw (brown line)—Drinkwater Basalt. Normal faults have ball and stick on hanging wall block.

Driving Instructions

Return to the vehicles and retrace the route westward ~20.2 miles to edge of the modern Harney Basin (S3-3). If there is not room to get off the road at this location, there is a turnout ~0.2 miles further west.

Stop 3-3. Westward Shift in the Loci of Extension and the Formation of the Harney Basin. (43.390°N, 118.491°W)

Three important observations can be made at Stop 3-3. First, differing depositional history across the Crane shear zone is indicated by contrasting stratigraphic sequences. North of the shear zone is a complete stratigraphic section, namely (1) fluvial and lacustrine sediment (Tts) that underlie the Devine Canyon Ash-Flow Tuff, (2) the Devine Canyon unit (Tdv), overlying sediment (Tst), and the Drinkwater Basalt (Tdw). South of the shear zone is the Steens Basalt (Tba), volcaniclastic strata, and the Drinkwater Basalt (Tdw) (Fig. 33). Secondly, varying degrees of extension north and south of the shear zone after emplacement of the Drinkwater Basalt suggests that the pattern of greater extension north of the shear zone persisted after the westward shift of deformation. Third, a vent for Drinkwater Basalt (Tdw) coincides (or occurs within) with the Crane shear zone. Similar relations between the Drinkwater Basalt and the Crane shear zone occur in the eastern part of the Crane basin, indicating that the shear zone localized the Tdw vents.

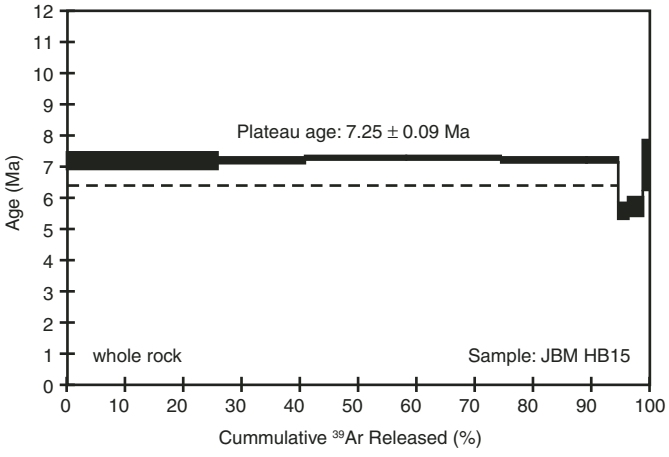

Figure 30 (Stop 3-1). $^{39}Ar/^{40}Ar$ age spectra for Tdw Drinkwater basalt sample JBM HB15 in east side of area (Fig. 28). From J. Milliard (unpublished).

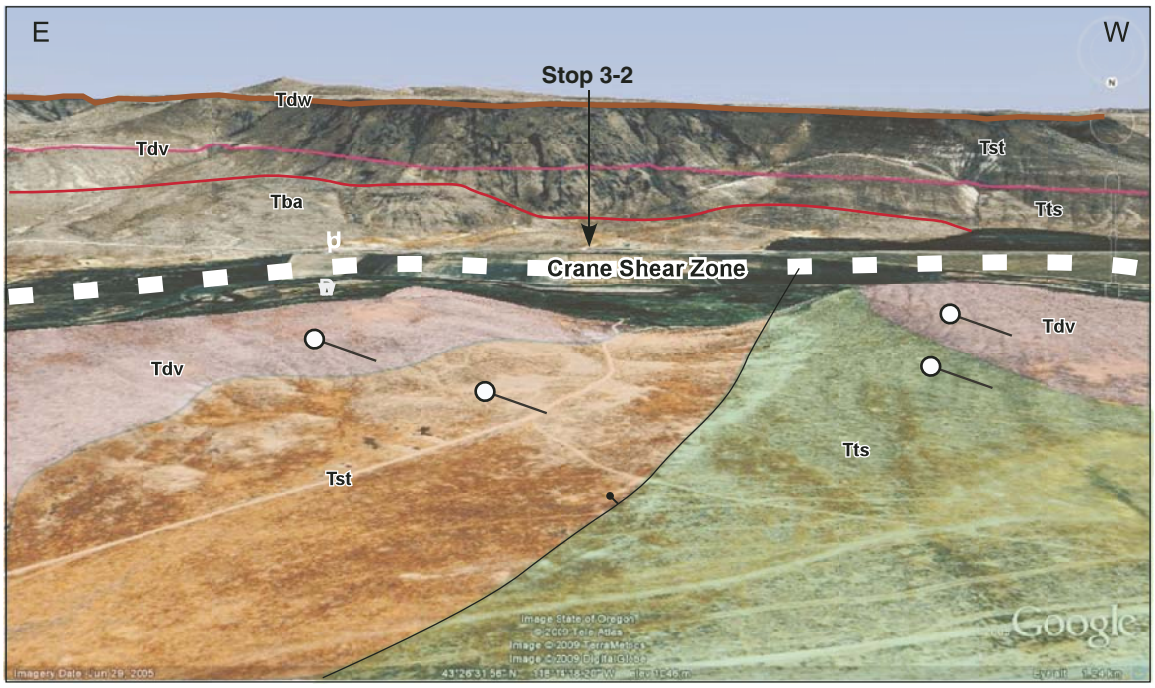

Figure 31 (Stop 3-2). Oblique view looking to the south toward Stop 3-2. Sticks with white balls indicate westward dip of strata in tilt blocks. The white thick dash line follows the valley bottom of the south fork of the Malheur River. Faults on the north side of the river do not continue to the south into the butte capped by the Drinkwater Basalt (Tdw; brown line). See Figure 29 figure caption for units.

Driving Instructions

The trip begins the return voyage to Portland, with one stop en route. Return to Burns and travel west on Highway 20 (toward Bend). Continue 4.9 miles west of Hampton (L3-2), turn right (north) on Lizard Creek Road, gravel (I3-2). Cougar Butte is the haystack-shaped butte to the northeast. As you drive off the basalt plain that is planted in alfalfa, the road traverses part of the Hampton Tuff, which has been dropped to this position on the hanging walls of a system of normal faults that form the southern edge of Hampton Buttes. Farther up the canyon, older buff-yellow tuffaceous sedimentary deposits are visible on the left side, beyond which are outcrops of hydrothermally altered and weathered rhyodacite. On the right, 4.4 miles from the highway as the road leaves the Lizard Creek canyon, is a small pullover adjacent to a quarry that exposes a section through the Hampton

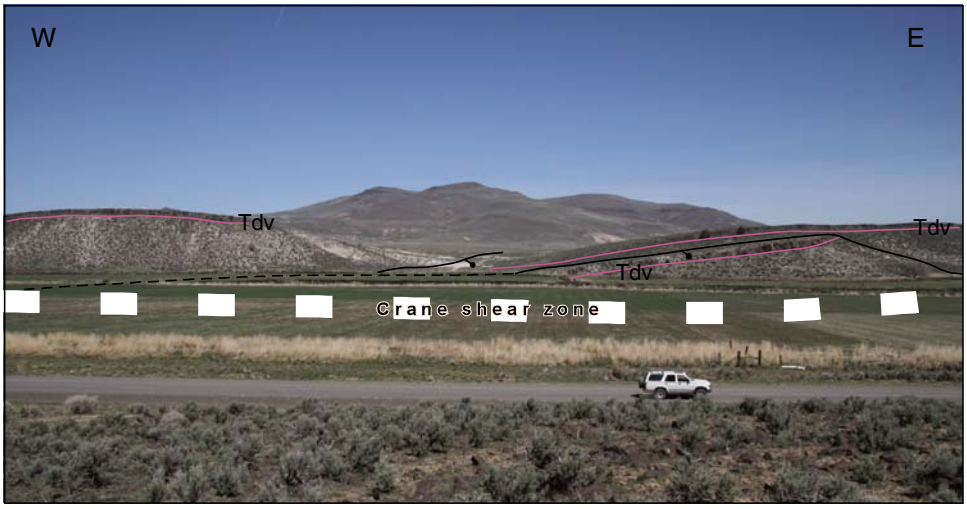

Figure 32 (Stop 3-2). View looking north from Stop 3-2. Photographer stands on the Steens Basalt. The two cuestas in the distance are capped by the Devine Canyon Ash-Flow Tuff. That stratum does not continue south across the Crane shear zone. See Figure 29 figure caption for units. The pink line marks the base of the Devine Canyon Tuff (Tdv) rim rock.

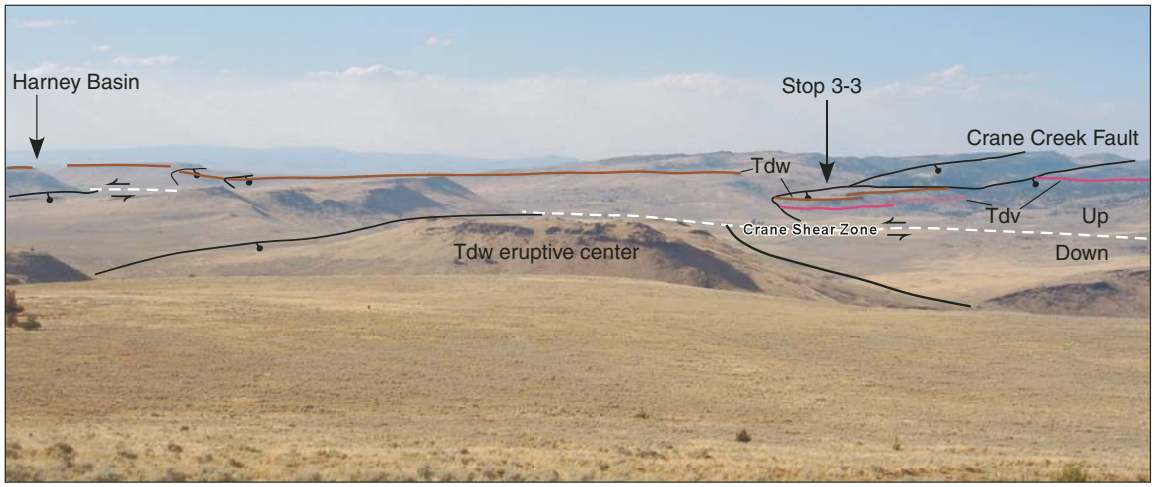

Figure 33 (Stop 3-3). View toward Stop 3-3 north showing major structures. Note that relatively large vertical separations characterize offset of the Drinkwater Basalt (Tdw). See Figure 29 figure caption for units.

Tuff. Continuing beyond the quarry, on the right side of the road a careful eye can find remains of the breccia that once covered the rhyodacite that forms the ridge that is also on the right side of the road. To the west, note the south-dipping basalts that pre-date the Hampton Tuff and lap onto the Hampton Butte edifice. Hampton Butte's steep east and west sides are the result of topographic inversion that occurred in Pliocene time. Breccia and pieces of the glassy carapace that once mantled the butte can be found on the uphill side of the hairpin turn in the road east. Continue on to the top of Hampton Butte (S3-4).

Stop 3-4 Lunch and Hampton Butte, the Northern Margin of the High Lava Plains (43.774°N, 120.281°W)

Hampton Butte and Cougar Butte are rhyodacite and dacite dome and flow complexes, respectively, with ages of 30.3 and 28.6 Ma (Fig. 34) (Iademarco, 2009). They are stratigraphically equivalent to the John Day Formation, expanding the known distribution of vents of that age and providing a bridge to volcanism of similar age units that crop out south of the High Lava Plains, such as the Coleman Hills (Scarberry et al., 2007). From the summit of Hampton Butte, green tuffaceous units visible to the north are part of the John Day Formation. To the south, in the distance, is the Basin and Range Province. Closer by, in the High Lava Plains, Frederick Butte lies 45° west of south, and Glass Buttes is 45° east of south. About 7.9 Ma, 3 km east of Hampton Butte, just beyond the small ridge of rhyodacite that extends from Hampton Butte toward Cougar Butte, a vent erupted andesite. a stack of shallowly south-dipping basalts onlap Hampton Butte rocks on the south side of butte. These basalts have ages of 7.7–7.8 Ma. These flows, together with the newly dated basalt of Dry Mountain (58 km to the east) at 7.9 Ma, are part of the ca. 8 Ma pulse of high-alumina olivine tholeiite that was widespread in the High Lava Plains. The contact between these basalts and the older volcanic basement defines the northern edge of the High Lava Plains, which also coincides with a scalloped edge to the distribution of densely spaced northwesterly faults of the Brothers fault zone. After ca. 3 Ma, volcanism recommenced in the Hampton Butte area with eruption of a basaltic andesite scoria vent (4.2 Ma) and the Hampton Tuff, a 3.8 Ma rhyolite ignimbrite presumably erupted from Frederick Butte. This phase of volcanism corresponds to the passage of the 4 Ma isochron of westward-younging silicic volcanism of the High Lava Plains. The Hampton Tuff laps unconformably onto the ca. 8 Ma basalt, which dips southward, and Hampton Butte indicating successive subsidence of the High Lava Plains.

End of the trip.

ACKNOWLEDGMENTS

Field trip guidebook editors Becky Dorsey, Ian Madin, and Jim O'Connor are thanked for their infinite patience and volunteer effort. Reviews by Scott Linneman and Dave Sherrod provided strong criticism and guidance that helped shape the final version of the manuscript. Dave Sherrod, in particular, went above and beyond the call of duty in his review. This research was support by National Science Foundation grants from the Continental Dynamics Program (EAR-0506869) and the Tectonics Program (EAR-0610064).

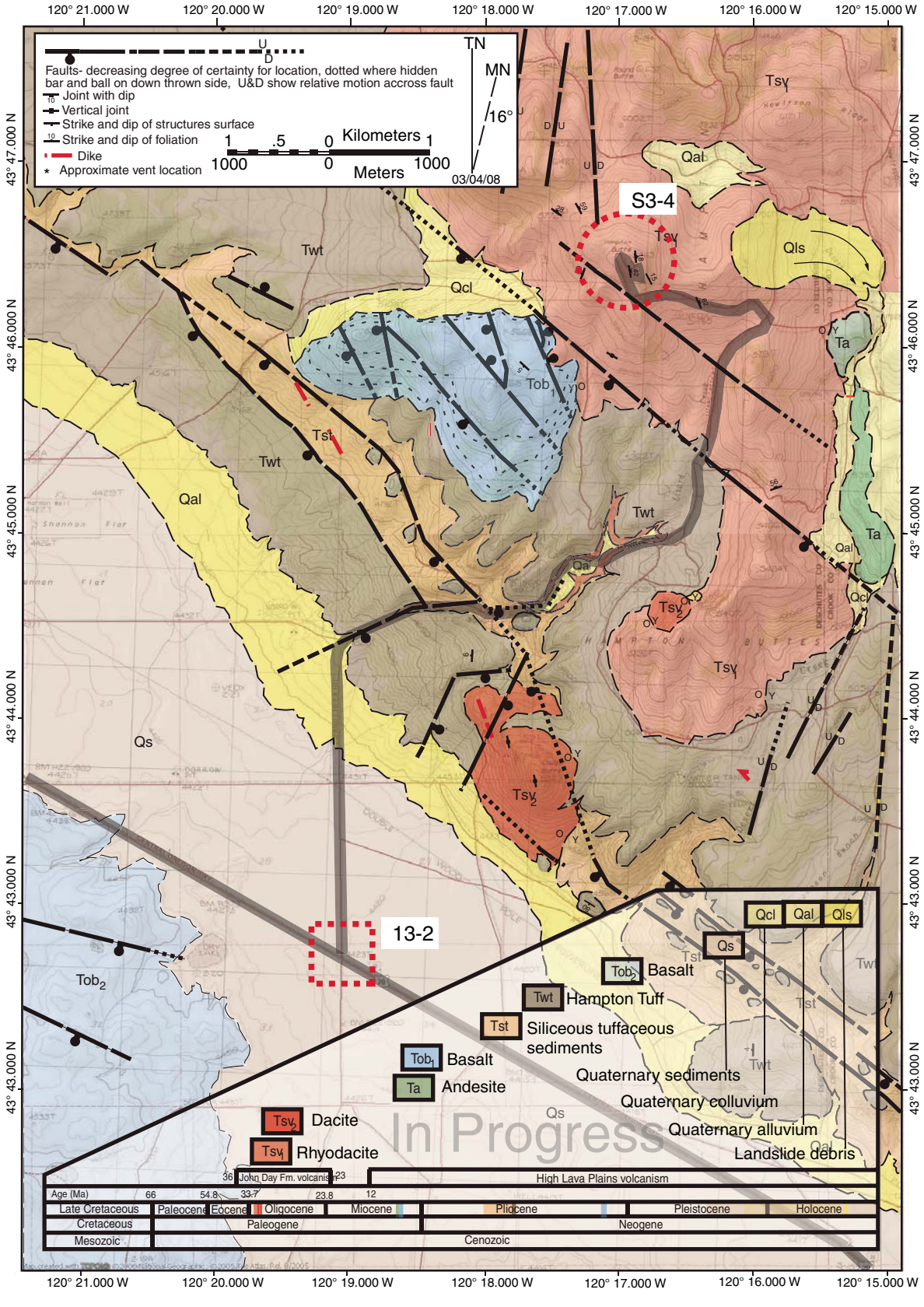

Figure 34 (Stop 3-4). Hampton Butte geologic map for Stop 3-4 (Fig. 27) Preliminary version that will form the basis of M. Iademarco's M.S. thesis.

REFERENCES CITED

Allison, I.S., 1982, Geology of Pluvial Lake Chewaucan, Lake County, Oregon: Corvallis, Oregon State University Press, 79 p.

Arestad, J.F., Potter, R.W., and Stewart, G.E., 1988, Stratigraphic test drilling in the Newberry Crater KGRA, Oregon: Geothermal Resources Council Bulletin, v. 17, p. 3–8.

Armstrong, R.L., and Ward, P., 1991, Evolving geographic patterns of the Cenozoic magmatism in the North American Cordillera: the temporal and spatial association of magmatism and metamorphic core complexes: Journal of Geophysical Research, v. 96, p. 13,201–13,224, doi: 10.1029/91JB00412.

Armstrong, R.L., Taubeneck, W.H., and Hales, P.O., 1977, Rb-Sr and K-Ar geochronometry of Mesozoic granitic rocks and the Sr isotopic composition, Oregon, Washington and Idaho: Geological Society of America Bulletin, v. 81, p. 3513–3536.

Atwater, T., and Stock, J., 1998, Pacific-North America Plate Tectonics of the Neogene Southwestern United States: An Update: International Geology Review, v. 40, p. 375–402, doi: 10.1080/00206819809465216.

Bachmann, O., and Bergantz, G.W., 2004, On the origin of crystal-pore rhyolites; extracted from batholithic crystal mushes: Journal of Petrology, v. 45, p. 1565–1582, doi: 10.1093/petrology/egh019.

Bacon, C.R., 2008, Geologic map of Mount Mazama and Crater Lake caldera, Oregon: U.S. Geological Survey Scientific Investigations Map, v. 2832.

Bacon, C.R., Bruggman, P.E., Christiansen, R.L., Clynne, M.A., Donnelly-Nolan, J.M., and Hildreth, W., 1997, Primitive magmas at five Cascades volcanic fields: melts from hot, heterogeneous sub-arc mantle: Canadian Mineralogist, v. 35, p. 397–423.

Badger, T.C., and Watters, R.J., 2004, Gigantic seismogenic landslides of Summer Lake basin, south-central Oregon: Geological Society of America Bulletin, v. 116, p. 687–697, doi: 10.1130/B25333.1.

Bartels, K.S., Kinzler, R.J., and Grove, T.L., 1991, High pressure phase relations of primitive high-alumina basalts from Medicine Lake volcano, northern California: Contributions to Mineralogy and Petrology, v. 108, p. 253–270, doi: 10.1007/BF00285935.

Bennett, R.A., Wernicke, B.P., Niemi, N.A., Friedrich, A.M., and Davis, J.L., 2003, Contemporary strain rates in the northern Basin and Range Province from GPS data: Tectonics, v. 22.

Best, M.G., and Christiansen, E.H., 1991, Limited extension during peak Tertiary volcanism, Great Basin of Nevada and Utah: Journal of Geophysical Research, v. 96, p. 13.

Brueseke, M.E., and Hart, W.K., 2008, Geology and petrology of the mid-Miocene Santa Rosa–Calico volcanic field, northern Nevada: Nevada Bureau of Mines and Geology Bulletin, v. 70, p. 343-360.

Brueseke, M.E., Heizler, M.T., Hart, W.K., and Mertzman, S.A., 2007, Distribution and geochronology of Oregon Plateau (U.S.A.) flood basalt volcanism; the Steens Basalt revisited: Journal of Volcanology and Geothermal Research, v. 161, p. 187–214, doi: 10.1016/j.jvolgeores.2006.12.004.

Camp, V.E., Ross, M.E., and Hanson, W.E., 2003, Genesis of flood basalts and Basin and Range volcanic rocks from Steens Mountain to the Malheur River Gorge, Oregon: Geological Society of America Bulletin, v. 115, p. 105–128, doi: 10.1130/0016-7606(2003)115<0105:GOFBAB>2.0.CO;2.

Carlson, R.W., and Hart, W.K., 1987, Crustal Genesis on the Oregon Plateau: Journal of Geophysical Research, v. 92, p. 6191–6208, doi: 10.1029/JB092iB07p06191.

Castor, S.B., and Henry, C.D., 2000, Geology, Geochemistry, and origin of volcanic rock-hosted uranium deposits in northwestern Nevada and southeastern Oregon, USA: Ore Geology Reviews, v. 16, p. 1–40, doi: 10.1016/S0169-1368(99)00021-9.

Catchings, R.D., and Mooney, W.D., 1988, Crustal structure of east central Oregon; relation between Newberry Volcano and regional crustal structure: Journal of Geophysical Research, v. 93, p. 10,081–10,094.

Christiansen, E.H., and McCurry, M., 2008, Contrasting origins of Cenozoic silicic volcanic rocks from the western Cordillera of the United States Bulletin of Volcanology, v. 70, p. 251–267.

Christiansen, R.L., and McKee, E.H., 1978, Late Cenozoic volcanic and tectonic evolution of the Great Basin and Columbia Intermontane regions, *in* Smith, R.B., and Eaton, G.P., eds., Cenozoic tectonics and regional geophysics of the western Cordillera: Geological Society of America Memoir 152, p. 283–311.

Christiansen, R.L., and Yeats, R.S., 1992, Post-Laramide geology of the U.S. Cordilleran region, *in* Burchfiel, B.C., Lipman, P.W., and Zoback, M.L., eds., The Cordilleran Orogen, Conterminous U.S.: Geological Society of America, Geology of North America, v. G-3, p. 261–406.

Christiansen, R.L., Evans, J.R., and Foulger, G.R., 2002, Upper-mantle origin of the Yellowstone Hotspot: Geological Society of America Bulletin, v. 114, p. 1245–1256, doi: 10.1130/0016-7606(2002)114<1245:UMOOTY>2.0.CO;2.

Colgan, J.P., Dumitru, T.A., McWilliams, M.O., and Miller, E.L., 2006, Timing of Cenozoic volcanism and Basin and Range extension in northwestern Nevada; new constraints from the northern Pine Forest Range: Geological Society of America Bulletin, v. 118, p. 126–139, doi: 10.1130/B25681.1.

Coney, P.J., and Reynolds, S.J., 1977, Cordilleran Benioff zones: Nature, v. 270, p. 403–406, doi: 10.1038/270403a0.

Conrad, W.K., 1984, The mineralogy and petrology of compositionally zoned ash flow tuffs, and related silicic volcanic rocks, from the McDermitt caldera complex, Nevada-Oregon: Journal of Geophysical Research, v. 89, p. 8639–8664, doi: 10.1029/JB089iB10p08639.

Conrey, R.M., Donnelly-Nolan, J.M., and Taylor, E.M., 2000, The north-central Cascade margin: exploring petrologic and tectonic intimacy in a propagating intra-arc rift: MARGINS 2000 Meeting Field Guide, p. 61.

Conrey, R.M., Sherrod, D.R., Hooper, P.R., and Swanson, D.A., 1997, Diverse, primitive magmas in the Cascade arc, northeast Oregon and southern Washington: Canadian Mineralogist, v. 35, p. 367–396.

Crider, J.G., 2001, Oblique slip and the geometry of normal-fault linkage: mechanics and case study from the Basin and Range in Oregon: Journal of Structural Geology, v. 23, p. 1997–2009, doi: 10.1016/S0191-8141(01)00047-5.

Davis, J.O., 1985, Correlation of Late Quaternary tephra layers in a long pluvial sequence near Summer Lake, Oregon: Quaternary Research, v. 23, p. 38–53, doi: 10.1016/0033-5894(85)90070-5.

Dickinson, W.R., 1979, Mesozoic forearc basin in central Oregon: Geology, v. 7, p. 166–170, doi: 10.1130/0091-7613(1979)7<166:MFBICO>2.0.CO;2.

Donath, F.A., 1962, Analysis of basin-range structure, south-central Oregon: Geological Society of America Bulletin, v. 73, p. 1–16, doi: 10.1130/0016-7606(1962)73[1:AOBSSO]2.0.CO;2.

Dugas, D.P., 1998, Late Quaternary variations in the level of paleo-Lake Malheur, eastern Oregon: Quaternary Research, v. 50, p. 276–282, doi: 10.1006/qres.1998.2005.

Ekren, E.B., McIntyre, D.H., Bennett, E.H., and Marvin, R.F., 1982, Cenozoic stratigraphy of western Owyhee County, Idaho, *in* Bonnichsen, B., and Breckenridge, R.M., eds., Cenozoic Geology of Idaho, Volume 26, Idaho Bureau of Mines Geology Bulletin, p. 215–235.

Faulds, J.E., and Varga, R.J., 1998, The role of accommodation zones and transfer zones in the regional segmentation of extended terranes, *in* Faulds, J.E., and Stewart, J.H., Accommodation Zones and Transfer Zones: The Regional Segmentation of the Basin and Range Province: Geological Society of America Special Paper 323, p. 1–45.

Faulds, J.E., Henry, C.D., and Hinz, N.H., 2005, Kinematics of the northern Walker Lane; an incipient transform fault along the Pacific-North American Plate boundary: Geology, v. 33, p. 505–508, doi: 10.1130/G21274.1.

Fiebelkorn, R.B., Walker, G.W., MacLeod, N.S., McKee, E.H., and Smith, J.G., 1983, Isochron/WestIndex to K-Ar determinations for the State of Oregon: Isochron/West, v. 37.

Ford, M.T., McCurry, M., and Chadwick, J., 2004, Genesis of Quaternary rhyolite domes of the eastern Snake River plain and Blackfoot volcanic field, SE Idaho: Geological Society of America Abstracts with Programs, v. 36, no. 4, p. 11.

Gans, P.B., Mahood, G.A., and Schermer, E.R., 1989, Synextensional magmatism in the Basin and Range Province; a case study from the eastern Great Basin: Geological Society of America Special Paper 233, 60 p.

Greene, R.C., 1973, Petrology of the welded tuff of Devine Canyon, southeastern Oregon: U.S. Geological Survey Professional Paper 797, p. 1–26.

Greene, R.C., Walker, G.W., and Corcoran, R.E., 1972, Geologic map of the Burns quadrangle, Oregon: Reston, Virginia, U.S. Geological Survey. Miscellaneous Geologic Investigations Map I-680.

Gudmundsson, A., Brynjolfsson, S., and Jonsson, M.T., 1993, Structural analysis of a transform fault-rift zone junction in North Iceland: Tectonophysics, v. 220, p. 205–221, doi: 10.1016/0040-1951(93)90232-9.

Hammond, W.C., and Thatcher, W., 2005, Northwest Basin and Range tectonic deformation observed with the Global Positioning System, 1999–2003: Journal of Geophysical Research, v. 110, p. 12.

Hart, W.K., 1985, Chemical and isotopic evidence for mixing between depleted and enriched mantle, northwestern U.S.A: Geochimica et Cosmochimica Acta, v. 49, p. 131–144, doi: 10.1016/0016-7037(85)90197-8.

Hart, W.K., Aronson, J.L., and Mertzman, S.A., 1984, Areal distribution and age of low-K, high-alumina olivine tholeiite magmatism in the northwestern Great Basin: Geological Society of America Bulletin, v. 95, p. 186–195, doi: 10.1130/0016-7606(1984)95<186:ADAAOL>2.0.CO;2.

Hildreth, W., 2004, Volcanological perspectives on Long Valley, Mammoth Mountain, and Mono Craters; several contiguous but discrete systems: Journal of Volcanology and Geothermal Research, v. 136, p. 169–198.

Hooper, P.R., Mahoney, J.J., and Coffin, M.F., 1997, The Columbia River flood basalt province: current status, Large Igneous Provinces: Washington, American Geophysical Union, p. 1–28.

Hooper, P.R., Binger, G.B., and Lees, K.R., 2002, Ages of the Steens and Columbia River flood basalts and their relationship to extension-related calc-alkalic volcanism in eastern Oregon: Geological Society of America Bulletin, v. 114, p. 43–50, doi: 10.1130/0016-7606(2002)114<0043:AOTSAC>2.0.CO;2.

Humphreys, E.D., 1995, Post-Laramide removal of the Farallon Slab: Western United States: Geology, v. 23, p. 987–990, doi: 10.1130/0091-7613(1995)023<0987:PLROTF>2.3.CO;2.

Humphreys, E.D., and Coblentz, D.D., 2007, North American dynamics and Western U. S. tectonics: Reviews of Geophysics, v. 45, RG3001, doi: 10.1029/2005RG000181.

Iademarco, M.J., 2009, Volcanism and Faulting along the Northern Margin of Oregon's High Lava Plains: Hampton Butte to Dry Mountain [M.S. thesis]: Corvallis, Oregon, Oregon State University, p. 150.

Jensen, R.A., 2006, Roadside guide to the geology and history of Newberry Volcano: Bend, Oregon, CenOreGeoPub, 182 p.

Jensen, R.A., Donnelly-Nolan, J.M., and Mckay, D.M., 2009, A field guide to Newberry Volcano, Oregon, *in* O'Connor, J.E., Dorsey, R.J., and Madin, I.P., eds., Volcanoes to Vineyards: Geologic Field Trips through the Dynamic Landscape of the Pacific Northwest: Geological Society of America Field Guide 15, doi: 10.1130/2009.fld015(03).

Johnson, J.A., 1995, Geologic evolution of the Duck Creek Butte eruptive center, High Lava Plains, southeastern Oregon [M.S. thesis]: Corvallis, Oregon, Oregon State university, 151 p.

Johnson, J.A., and Grunder, A.L., 2000, The making of intermediate composition magma in a bimodal suite; Duck Butte eruptive center, Oregon, USA: Journal of Volcanology and Geothermal Research, v. 95, p. 175, doi: 10.1016/S0377-0273(99)00125-0.

Johnson, J.A., Hawkesworth, C.J., Hooper, P.R., and Binger, G.B., 1998, Major- and trace-element analyses of Steens Basalt, southeastern Oregon: U.S. Geological Survey Open-File Report 0196-1497, p. 30.

Jónasson, K., 2007, Silicic volcanism in Iceland: Composition and distribution within the active volcanic zones: Journal of Geodynamics, v. 43, p. 101–117, doi: 10.1016/j.jog.2006.09.004.

Jordan, B.T., Streck, M.J., and Grunder, A.L., 2002, Bimodal volcanism and tectonism of the High Lava Plains, Oregon: Oregon Department of Geology and Mineral Industries, Special Paper, v. 36, p. 23.

Jordan, B.T., Grunder, A.L., Duncam, R.A., and Deino, A.L., 2004, Geochronology of age-progressive volcanism of the Oregon High Lava Plains: Implications for the plume interpretation of Yellowstone: Journal of Geophysical Research, v. 109, B10202, doi: 10.1029/2003JB002776.

Keller, G.R., Hildenbrand, T.G., Kucks, R., Roman, D., and Hittleman, A.M., 2002, Upgraded gravity anomaly base of the United States: Leading Edge, v. 21, p. 366–367, doi: 10.1190/1.1471598.

Langer, V.W., 1991, Geology and petrologic evolution of silicic and intermediate volcanic rocks underneath Steens Mountain Basalt, SE Oregon [M.S. Thesis]: Corvallis, Oregon State University, 109 p.

Langridge, R., Pezzopane, S., and Weldon, R., 2001, Slip rate, recurrence intervals, and paleoearthquakes for the Ana River Fault, central Oregon, *in* Negrini, R., Pezzopane, S., and Badger, T., eds., Quaternary Studies near Summer Lake, Oregon: Bakersfield, Friends of the Pleistocene, Pacific Northwest Cell, p. RL1–12.

Lawrence, R.D., 1976, Strike-slip faulting terminates the Basin and Range Province in Oregon: Geological Society of America Bulletin, v. 87, p. 846–850, doi: 10.1130/0016-7606(1976)87<846:SFTTBA>2.0.CO;2.

Leeman, W.P., 1982, Olivine tholeiitic basalts of the Snake River Plain, Idaho, *in* Bonnichsen, B., and Breckenridge, R.M., eds., Cenozoic Geology of Idaho: Idaho Bureau of Mines and Geology Bulletin, v. 26, p. 181–191.

Lerch, D.W., Miller, E., McWilliams, M., and Colgan, J., 2008, Tectonic and magmatic evolution of the northwestern Basin and Range and its transition to unextended volcanic plateaus: Black Rock Range, Nevada: Geological Society of America Bulletin, v. 120, p. 300–311, doi: 10.1130/B26151.1.

Lipman, P.W., Prostka, H.J., and Christiansen, R.L., 1972, Cenozoic volcanism and plate tectonic evolution of the western United States, I: Philosophical Transactions of the Royal Society of London. Series A: Mathematical and Physical Sciences, v. 271, p. 217–248, doi: 10.1098/rsta.1972.0008.

Luedke, R.G., and Smith, R.L., 1984, Map showing distribution, composition, and age of late Cenozoic volcanic centers in the western conterminous United States: U.S. Geological Survey Miscellaneous Investigations Series Map I-1523, scale 1:2,500,000.

MacLeod, N.S., Walker, G.W., and McKee, E.H., 1975, Geothermal significance of eastward increase in age of upper Cenozoic rhyolitic domes in southeastern Oregon: U.S. Geological Survey Open-File Report 75-034, 21 p.

MacLeod, N.S., Sherrod, D.R., Chitwood, L.A., and Jensen, R.A., 1995, Geologic map of Newberry volcano, Deschutes, Klamath, and Lake counties, Oregon: U.S. Geological Survey Miscellaneous Investigations Map I2455, scale 1:62,500 and 1:24,000.

Manduca, C.A., Silver, L.T., and Taylor, H.P., 1992, $^{87}Sr/^{86}Sr$ and $^{18}O/^{16}O$ isotopic systematics and geochemistry of granitoid plutons across a steeply-dipping boundary between contrasting lithospheric blocks in western Idaho: Contributions to Mineralogy and Petrology, v. 109, p. 355–372, doi: 10.1007/BF00283324.

Mankinen, E.A., Larson, E.E., Gromme, C.S., Prevot, M., and Coe, R.S., 1987, The Steens Mountain (Oregon) geomagnetic polarity transition; 3, Its regional significance: Journal of Geophysical Research, v. 92, p. 8057–8076, doi: 10.1029/JB092iB08p08057.

Mathis, A.C., 1993, Geology and petrology of a 26-Ma trachybasalt to peralkaline rhyolite suite exposed at Hart Mountain, southern Oregon [M.S. thesis]: Corvallis, Oregon State University, 141 p.

McCaffrey, R., Long, M.D., Goldfinger, C., Zwick, P.C., Nabelek, J.L., Johnson, C.K., and Smith, C., 2000, Rotation and plate locking at the southern Cascadia subduction zone: Geophysical Research Letters, v. 27, p. 3117–3120, doi: 10.1029/2000GL011768.

McCurry, M., Hayden, K.P., Morse, L.H., and Mertzman, S., 2008, Genesis of post-hotspot, A-type rhyolite of the Eastern Snake River Plain volcanic field by extreme fractional crystallization of olivine tholeiite: Bulletin of Volcanology, v. 70, p. 361–383, doi: 10.1007/s00445-007-0143-4.

McDonough, W.F., and Sun, S.-s., 1995, The composition of the Earth: Chemical Geology, v. 120, p. 223–253, doi: 10.1016/0009-2541(94)00140-4.

McKee, E.H., Duffield, W.A., and Stern, R.J., 1983, Late Miocene and early Pliocene basaltic rocks and their implications for crustal structure, northeastern California and south-central Oregon: Geological Society of America Bulletin, v. 94, p. 292–304, doi: 10.1130/0016-7606(1983)94<292:LMAEPB>2.0.CO;2.

Miller, M.M., Dixon, T.H., Dokka, R.K., and Johnson, D.J., 2001, Refined kinematics of the Eastern California shear zone from GPS observations, 1993–1998: Journal of Geophysical Research, v. 106, p. 2245–2263, doi: 10.1029/2000JB900328.

Minor, S.A., Plouff, D., Esparaza, L.E., and Peters, T.J., 1987, Mineral resources of the High Steens and Little Blitzen Gorge Wilderness Study Areas, Harney County, Oregon: U.S. Geological Survey Bulletin 8755-531X p. A1–A21.

Oldow, J.S., Carlson, R.L., and Kobayashi, K., 1984, Evolution of a late Mesozoic back-arc fold and thrust belt, northwestern Great Basin, U.S.A: Geodynamics of back-arc regions, v. 102, p. 245–274.

Peterson, N.V., and Groh, E.A., 1964, Crack-in-the-Ground, Lake County, Oregon: Oregon Department of Geology and Mineral Industries: Portland, Oregon, Ore Bin, v. 26, p. 158–166.

Pezzopane, S., 2001, Pluvial Lake Chewaucan shoreline elevations, *in* Negrini, R., Pezzopane, S., and Badger, T., eds., Quaternary Studies near Summer Lake, Oregon: Bakersfield, Friends of the Pleistocene, Pacific Northwest Cell, p. SP1–5.

Pezzopane, S.K., and Weldon, R.J., II, 1993, Tectonic role of active faulting in central Oregon: Tectonics, v. 12, p. 1140–1169.

Pierce, K.L., and Morgan, L.A., 1992, The track of the Yellowstone hot spot: Volcanism, faulting, and uplift, *in* Link, P.K., Kuntz, M.A., and Platt, L.B., eds., Regional Geology of Eastern Idaho and Western Wyoming: Geological Society of America Memoir 179, p. 1–53.

Pierce, K.L., Morgan, L.A., and Saltus, R.W., 2000, Yellowstone plume head: postulated tectonic relations to the Vancouver slab, continental boundaries, and climate: U.S. Geological Survey Open File Report 2000-498, p. 25.

Roth, J.B., Fouch, M.J., James, D.E., and Carlson, R.W., 2008, 3D seismic velocity structure of the northwestern United States: Geophysical Research Letters, v. 35, p. L15304, doi: 10.1029/2008GL034669.

Russell, J.K., Nixon, G.T., and Pearce, T.H., 1988, Petrographic constraints on modelling the crystallization of basalt magma, Cow Lakes, Southeast Oregon: Canadian Journal of Earth Sciences (Revue Canadienne des Sciences de la Terre), v. 25, p. 486–494.

Rytuba, J.J., and McKee, E.H., 1984, Peralkaline ash flow tuffs and calderas of the McDermitt volcanic field, Southeast Oregon and north central Nevada: Journal of Geophysical Research, v. 89, p. 8616–8628.

Scarberry, K., Grunder, A., and Meigs, A., 2007, Transition from intermediate to bimodal volcanism and inception and style of extensional faulting within the margin of the basin and range province, southern Oregon: Eos (Transactions, American Geophysical Union), v. 88.

Scarberry, K., Meigs, A., and Grunder, A., 2009, Inception and style of faulting at the edge of a propagating continental rift system: Insight from the structural development of the Abert Rim fault, southern Oregon: Tectonophysics (in press).

Seedorff, E., Raines, G.L., Lisle, R.E., Schafer, R.W., and Wilkinson, W.H., 1991, Magmatism, extension, and ore deposits of Eocene to Holocene age in the Great Basin; mutual effects and preliminary proposed genetic relationships Geology and ore deposits of the Great Basin; symposium proceedings: Reno, Nevada, Geological Society of Nevada, p. 133–178.

Sherrod, D.R., and Smith, J.G., 1990, Quaternary extrusion rates of the Cascade Range, northwestern Unites States and southern British Columbia: Journal of Geophysical Research, v. 95, p. 19465–19747, doi: 10.1029/JB095iB12p19465.

Sherrod, D.R., Mastin, L.G., Scott, W.E., and Schilling, S.P., 1997, Volcano hazards at Newberry volcano, Oregon: U.S. Geological Survey Open-File Report 97-513, 14 p.

Shoemaker, K.A., and Hart, W.K., 2001, Time-space patterns of basaltic volcanism on the Owyhee Plateau, Oregon-Nevada-Idaho: Geological Society of America Abstracts with Programs, v. 33, no. 6, p. 139.

Stewart, J.H., and Carlson, J.E., 1974, Preliminary geologic map of Nevada, U.S. Geological Survey Miscellaneous Field Studies Map, MF-609, scale 1:500,000.

Streck, M.J., 2002, Partial melting to produce high-silica rhyolites of a young bimodal suite; compositional constraints among rhyolites, basalts, and metamorphic xenoliths from the Harney Basin, Oregon: Berlin, Federal Republic of Germany, Springer International, Geologische Rundschau (International Journal of Earth Sciences), v. 91, p. 583–593.

Streck, M.J., and Grunder, A.L., 1995, Crystallization and welding variations in a widespread ignimbrite sheet; the Rattlesnake Tuff, eastern Oregon, USA: Bulletin of Volcanology, v. 57, p. 151–169.

Streck, M.J., and Grunder, A.L., 1997, Compositional gradients and gaps in high-silica rhyolites of the Rattlesnake Tuff, Oregon: Journal of Petrology, v. 38, p. 133–163, doi: 10.1093/petrology/38.1.133.

Streck, M.J., and Grunder, A.L., 1999, Enrichment of basalt and mixing of dacite in the rootzone of a large rhyolite chamber: inclusions and pumices from the Rattlesnake Tuff, Oregon: Contributions to Mineralogy and Petrology, v. 136, p. 193–212, doi: 10.1007/s004100050532.

Streck, M.J., and Grunder, A.L., 2008, Phenocryst-poor rhyolites of bimodal, tholeiitic provinces: the Rattlesnake Tuff and implications for mush extraction models: Bulletin of Volcanology, v. 70, p. 385–401, doi: 10.1007/s00445-007-0144-3.

Suppe, J., Powell, C., and Berry, R., 1975, Regional topography, seismicity, Quaternary volcanism, and the present day tectonics of the western United States: American Journal of Science, v. 275A, p. 397–417.

Trehu, A.M., Asudeh, I., Brocher, T.M., Luetgert, J.H., Mooney, W.D., Nabelek, J.L., and Nakamura, Y., 1994, Crustal architecture of the Cascadia Forearc: Science, v. 266, p. 237–243, doi: 10.1126/science.266.5183.237.

Trench, D., 2008, The Termination of the Basin and Range Province into a Clockwise Rotating Region of Transtension and Volcanism, Central Oregon [M.S. thesis]: Corvallis, Oregon State University, 64 p.

Vallier, T.L., 1995, Petrology of pre-Tertiary igneous rocks in the Blue Mountains region of Oregon, Idaho, and Washington; implications for the geologic evolution of a complex island arc: U.S. Geological Survey Professional Paper 1438, p. 125–209.

Walker, G.W., 1979, Revisions to the Cenozoic stratigraphy of Harney Basin, southeastern Oregon: U.S. Geological Survey Bulletin 1475, 35 p.

Walker, G.W., and MacLeod, N.S., 1991, Geologic Map of Oregon: Denver, U.S. Geological Survey, scale: 1:500,000.

Wells, R.E., 1980, Drake Peak; a structurally complex rhyolite center in southeastern Oregon: U.S. Geological Survey Professional Paper 1124, p. E1–E16.

Wells, R.E., and Heller, P.L., 1988, The relative contribution of accretion, shear, and extension to Cenozoic tectonic rotation in the Pacific Northwest: Geological Society of America Bulletin, v. 100, p. 325–338, doi: 10.1130/0016-7606(1988)100<0325:TRCOAS>2.3.CO;2.

Wells, R.E., and Simpson, R.W., 2001, Northward migration of the Cascadia forearc in the northwestern U.S. and implications for subduction deformation: Earth, Planets, and Space, v. 53, p. 275–283.

Wells, R.E., Weaver, C.S., and Blakely, R.J., 1998, Fore arc migration in Cascadia and its neotectonic significance: Geology, v. 26, p. 759–762, doi: 10.1130/0091-7613(1998)026<0759:FAMICA>2.3.CO;2.

Wernicke, B.P., 1992, Cenozoic extensional tectonics of the U.S. Cordillera *in* Burchfiel, B.C., Lipman, P.W., and Zoback, M.L., eds., Cordilleran Orogen; conterminous U.S.: Geological Society of America, Geology of North America, v. G-3, p. 553–581.

Wesnousky, S.G., 2005, Neotectonics and contemporary strain accumulation across the Walker Lane and northern Great Basin, USA: Eos (Transactions, American Geophysical Union), v. 86 p. g51d.

Whitaker, M.L., Nekvasil, H., Lindsley, D.H., and McCurry, M., 2008, Can crystallization of olivine tholeiite give rise to potassic rhyolites? An experimental investigation: Bulletin of Volcanology, v. 70, p. 417–434, doi: 10.1007/s00445-007-0146-1.

Zandt, G., and Humphreys, E., 2008, Toroidal mantle flow through the Western U.S. slab window: Geology, v. 36, p. 295–298, doi: 10.1130/G24611A.1.

Zoback, M.L., 1989, State of stress and modern deformation of the northern Basin and Range Province Journal of Geophysical Research, v. 94, p. 7105–7128.

Zoback, M.L., McKee, E.H., Blakely, R.J., and Thompson, G.A., 1994, The northern Nevada rift: regional tectono-magmatic relations and Middle Miocene stress direction: Geological Society of America Bulletin, v. 106, p. 371–382, doi: 10.1130/0016-7606(1994)106<0371:TNNRRT>2.3.CO;2.

Manuscript Accepted by the Society 17 July 2009